THE UNIVERSITY OF ADELAIDE

THE GEOLOGY, PETROLOGY AND GEOCHEMISTRY
OF THE VOLCANICS IN THE KOKATHA REGION,
GAWLER RANGES, SOUTH AUSTRALIA.

by BENJAMIN D. ROBERTSON B.Sc.

November, 1989

C

THE GEOLOGY, PETROLOGY AND GEOCHEMISTRY OF THE

VOLCANICS IN THE KOKATHA REGION, GAWLER RANGES,

SOUTH AUSTRALIA.

by Benjamin D. Robertson

Thesis submitted as partial fulfilmentfor the

Honours Degree of Bachelor of Science.

Department of Geology and Geophysics

University of Adelaide

November, 1989.

National Grid Reference   SH   53-15   (1:250000)

3

CONTENTS

CONTENTS (continued)

LIST OF APPENDICES

LIST OF TABLES AND FIGURES INCLUDED IN THE TEXT

Tables

Figures

Figures   (cont)

ABSTRACT

Volcanics in the Kokatha region present a wider range of rock types than in other areas of the Gawler Ranges. High temperature Mg rich basalt flows through to rhyolite ignimbrites and air fall tuffs outcrop. Two magmatic cycles are observed with a cycle consisting of initial basalts, followed by voluminous dacites and rhyodacites. The final phase of the cycle following the rhydacites represents a period of more explosive activity resulting in the deposition of rhyolitic ignimbrites, air fall tuffs rhyolitic flows and pyroclastics.

Geochemical data indicate both fractionation and mixing of fractionated components were active igneous processes resulting in the formation of layered magma chambers. The layering of the magma chambers being well illustrated in the stratigraphy of the volcanic pile. Further evidence for cyclic fractionation trends exists, with a relative depletion of incompatible elements in the second cycle when compared to the first cycle. Discrimination diagrams plot the rocks from Kokatha in the calc-alkaline field. Calc-alkaline series usually indicate subduction processes however volcanism at Kokatha is intracratonic.

Rb-Sr data give an isochron age of 1588.4 ± 14 Ma suggesting the rocks from Kokatha are a part of the lower sequence of the Gawler Range Volcanics. Samples from both cycles produce the isochron indicating a melt from a homogeneous source.

Neodymium data suggests a basaltic input from the mantle assimilating with lower crust is a likely source.

A possible tectonic model for volcanism is presented. Initially a flux of mantle derived basalt enters the lower crust. This provides heat for large scale melting. Assimilation of lower

crustal melts and mantle derived basalts may or may not occur however a homogeneous source is formed. Diaparism resulting in upper crustal magma chambers allows the formation of a layered magma chamber. Eruption of the magma reults in the stratigraphic sequence of volcanic rock units.

CHAPTER 1 INTRODUCTION

1.1 LOCATION OF STUDY AREA

The location of this study is centred on well exposed outcrops of volcanics immediately surrounding Kokatha Homestead (fig.1). The area is one of the most northern outcrops of the Gawler Range Volcanics, being situated approximately 50 Km south of Kingoonya.

1.2 PREVIOUS INVESTIGATIONS

Earlier work in the Kokatha region has been carried out in main by Blissett (1975) and Branch (1978).

Blissett (1975) in his regional reconnaissance described a series of volcanic units, stacked in an easterly direction dipping between 15 and 30 degrees. These units he ascribed to the Chitanilga Volcanic Complex. Overlying to the east is a thick dacite unit known as the Chandabooka Dacite (Blissett,1975).

Branch (1978) described the area as somewhat more complex. He proposed a caldera complex model based on the Cainozoic ignimbrite provinces in the western U.S.A.

1.3 AIMS OF STUDY

(1)   To map and sample the field area.

(2)   A petrological and geochemical study of rock types.

(3)   To seek evidence for hydrothermal activity.

(4)   Sr/Rb and Sm/Nd isotopes for age determination and possible source of crustal melting.

(5)   Model for volcanism.

1.4 METHODS OF STUDY

(1) Field mapping by foot using 1:20000 colour aerial photograph blown up from 1:87500.

(2) Petrographic examination of 27 thin and polished thin sections.

(3) Whole rock analysis of 54 samples.

(4) Electron microprobe analysis of 7 polished thin sections.
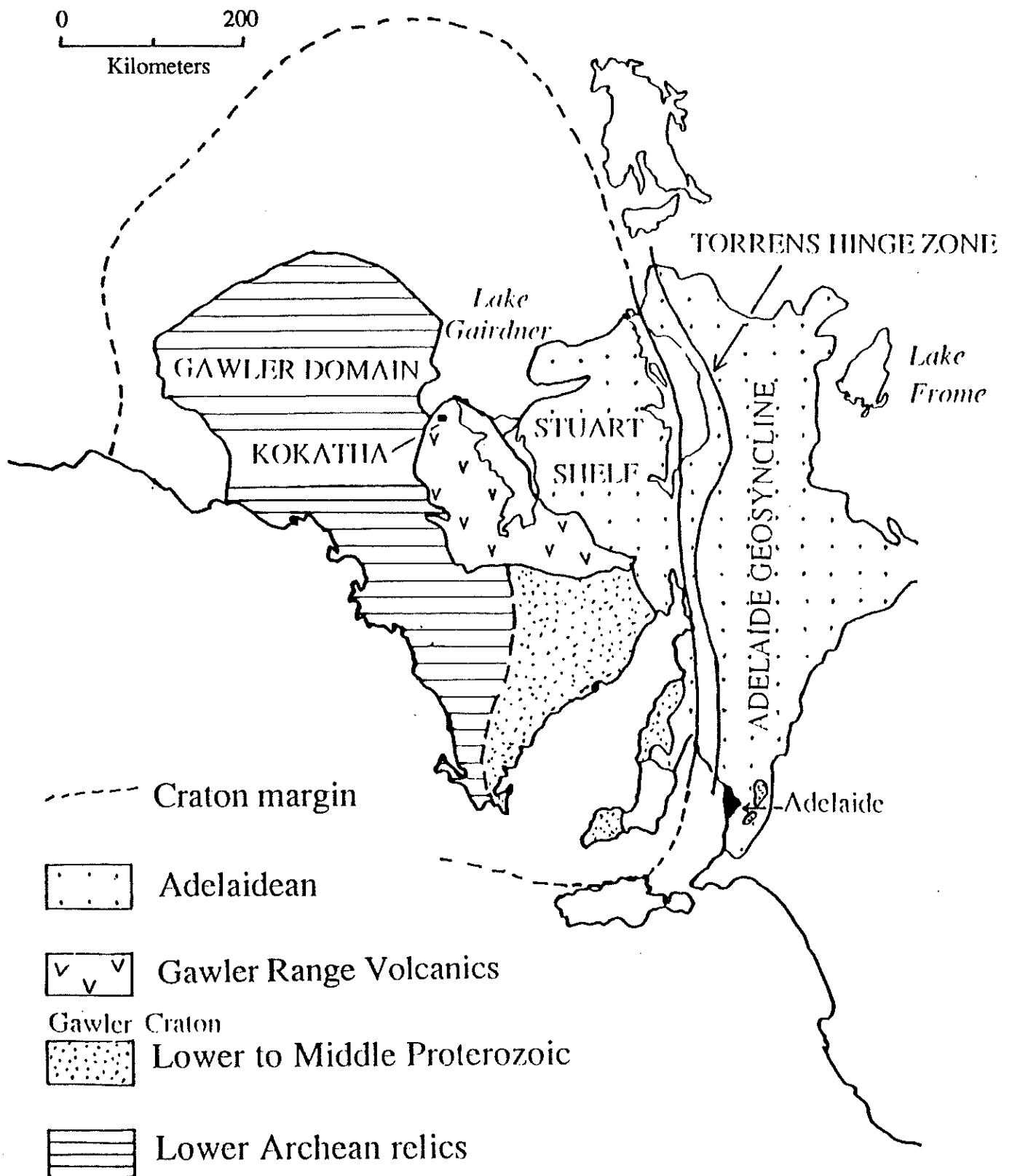
FIGURE 1   Map showing location of study area and regional South
Australian geology.

CHAPTER 2 REGIONAL GEOLOGY

2.1 GAWLER CRATON

The Gawler Craton comprises much of Eyre Peninsula in South Australia forming an extensive shield (fig.1). It is comprised of Precambrian crystalline basement which has remained stable except for local epeirogenic movements since approximately 1450 Ma (Fanning et al.,1988). It is bounded to the east by the Torrens Hinge Zone and Adelaide fold belt, to the north northwest by the Officer Basin and to more recent basins formed by faulting associated with the Mesozoic separation of Australia and Antartica, to the south and southwest (Parker et al.,1981).

Archean to Early Proterozoic rocks of the Sleafordian and Mulgathing Complexes form the basement rocks to the craton (fig.2). Both complexes consist of folded gneisses which probably represent strongly metamorphosed sediments over at least 2 deformational periods. Intruded into these metamorphosed sediments are granites which signify the ending of the Sleafordian Orogeny (Webb et al., 1986).

A period of tectonic quiescence followed the Sleafordian Orogeny, which resulted in the deposition of the Hutchinson Group. Iron formations and the Warrow Quartzite of this group outcrop in the eastern part of the craton forming the Middleback Ranges near Whyalla. Both groups, the Sleaford and Mulgathing complexes and the Hutchison Group were deformed by a multi-deformation orogeny known as the Kimban Orogeny. During this orogeny at least 3 phases of intrusives were emplaced (Lincoln Complex) along with extrusive rocks including the Myola Volcanics and Moonabie Formation McGregor Volcanics.

2.2 GAWLER RANGE VOLCANICS

The Gawler Range Volcanics are essentially undeformed extensive sheets of ignimbrites and lava flows covering an area of some 25000 km^2. They outcrop over the northern part of Eyre Peninsula forming the prominant hills of the Gawler Ranges. The volcanics were extruded following the Kimban Orogeny and can be divided into younger and older sequences (Blissett & Radke, 1979). The younger sequences consist predominantly of porphyritic dacite and rhyodacite whereas older volcanics as in the Kokatha and Glyde Hill regions include more basic rocks as well as rhyolites and dacites.

2.3 STUART SHELF

The Stuart Shelf occurs on the eastern margin of the Gawler Craton (fig.1) and is separated from the deformed sediments of the Adelaide Geosyncline by the Torrens Hinge Zone. The shelf is characterized by accumulations of sediments on top of basement with sedimentation being controlled by block faulting. The sedimentary units are undeformed distinguishing themselves from those east of the Torrens Hinge Zone.

2.4 GEOCHRONOLOGY

2.4.1 INTRODUCTION

Dating of rocks within the Gawler Craton using both Rb-Sr and U-Pb methods has been undertaken by a series of authors. Rb-Sr whole rock isochrons have been produced by Cooper et al.(1976), Webb and Thomson (1977), Daly et al.(1978) and Webb et al.(1986). U-Pb zircon geochronology has been investigated in more recent years by Cooper et al.(1985). Mortimer et al.(1986) and Fanning et al.

(1988). Rb-Sr geochronology is thought to be more susceptible to alteration effects (Fanning et al.,1988) with increasing susceptibility towards the Torrens Hinge Zone. However, for most of the Gawler Craton Rb-Sr isochrons are acceptable.

Figure 2 summarises ages, orogenic events and rock types of the Gawler Craton.

2.4.2 SLEAFORD AND MULGATHING COMPLEXES

The Sleaford and Mulgathing Complexes are constrained to be the oldest rocks of the craton with Rb-Sr isotopic ages for intrusive rocks such as the Glenloth Granite (Mulgathing) giving an age of 2350 ± 33 Ma (Webb & Thomson, 1977). Other intrusives such as the Dutton Suite Granitoids in Sleaford complex include all 2300-2500 Ma granitoid intrusives on southern Eyre Peninsula (Webb et al.,1986). Depending on various definitions of the Archean-Proterozoic boundary, the gneisses in which the granitoid bodies intrude can be said to be Archean in age (the arbitrary value of 2500 Ma has been proposed by the IUGS subcommission on Precambrian stratigraphy (Sims,1979)).

2.4.3 HUTCHISON GROUP

The third time division (fig.2), following the initial deposition of Archean sediments and Sleaford Orogeny, is defined as the interval from 2300 Ma to 1820 Ma (Webb, 1980a). The Hutchison Group, including the Warrow Quartzite and iron formations of the Middleback Ranges, were deposited during a period of relative tectonic quiescence (Parker & Lemon, 1982).

2.4.4 KIMBAN OROGENY

The Kimban Orogeny marks the fourth time division of the

Gawler Craton (fig.2 ; Webb et al.,1986). The time interval extending from 1820 Ma to 1580 Ma (Webb, 1980a). Rb-Sr isochron ages of both metamorphic and intrusive rocks tend to suggest at least three phases of activity occurred during the orogeny (Webb et al.,1986). Early activity included the intrusion of the Donnington Igneous Suite dated at 1818 ± 13 Ma (Mortimer et al.,1986). Other phases of activity between 1700 and 1600 Ma are recorded with a metamorphic age from samples at Mt. Woods giving an upper age of 1577 ± 92 for the orogeny (Webb et al.,1986).

2.4.5 GAWLER RANGE VOLCANICS

At the termination of the Kimban Orogeny, large scale magmatism resulted in the extrusion of the Gawler Range Volcanics and the later intrusion of the Hiltaba Granite. This was preceded, however by minor acid and basic igneous activity during the last stages of the Kimban Orogeny (Webb et al.,1986). Dominantly acid volcanics in the Moonabie Range (McGregor Volcanics) have been dated at 1615 ± 29 and 1645 ± 15 Ma (Webb et al.,1986) with the 1615 ± 29 Ma regarded as the more representative age of volcanism.

The earliest volcanics attributed to the Gawler Range Volcanics occur in the northern parts of the province. Rb-Sr isotopic age for the Chandabooka Dacite near Kokatha have given an age of 1525 ± 14 Ma with ages from the Glyde Hill Volcanic Complex being indistinguishable from this result (Webb et al.,1986). Similarities between the basal volcanics (Kokatha) and the McGregor Volcanics of the Moonabie Range plus the suggestion that sediments synchronous with early Gawler Range Volcanics in the Corunna and Tarcoola regions are older than 1550 Ma indicates the lower Gawler Range Volcanics may be somewhat older than 1525 Ma (Webb et al.,1986).

The most widespread event of the Gawler Range Volcanics was the extrusion of the Yardea Dacite. Rb-Sr analysis gives an age of 1529 ± 33 Ma (Webb et al.,1986), which should be noted to predate the Rb-Sr isochron ages for inferred underlying lower Gawler Range Volcanics. U-Pb ages for zircons in Yardea Dacite gives values of 1592 ± 3 Ma (Fanning et al.,1988). This age is significantly older than the Rb-Sr isochron age of 1529 ± 33 Ma. Fanning et al. (1988) suggests this difference can be attributed to deuteric alteration or a younger heating event which tends to decrease the isochron age in Rb-Sr systematics.

2.4.6 HILTABA GRANITE

Following the main volcanic activity the intrusion of a series of high level granites known as the Hiltaba Suite occurred. Samples from "Kokatha" and "Hiltaba" define a Rb-Sr isochron age of 1478 ± 38 Ma (Webb et al.,1986). Hiltaba Granite in the Tarcoola region gives Rb-Sr ages of 1475 ± 45 Ma (Webb et al.,1986). U-Pb zircon geochronology by Cooper et al.(1985) indicates, however, plutonism occurred earlier at 1514 ± 16 Ma.

2.4.7 CRATONIZATION

Cratonization of the Gawler Craton essentially defines the time when large scale tectonism ceased at around 1450 Ma (Parker et al.,1985). Immediately preceeding cratonization tectonism known as the Wartakan Event affected most of the region. Evidence for the Event is in the form of largescale warping, crossfolding and fracturing of not only basement but also the Corunna beds. Cratonization followed this Event. Deposition of sediments in grabens and dolerite dyke intrusion during the Late Proterozoic are examples of intracratonic tensional processes (Parker et al.,1985).

AGE		OROGENIC EVENTS	SUPRACRUSTAL ROCKS	INTRUSIVE ROCKS
	Ma	6	CRATONISATION	
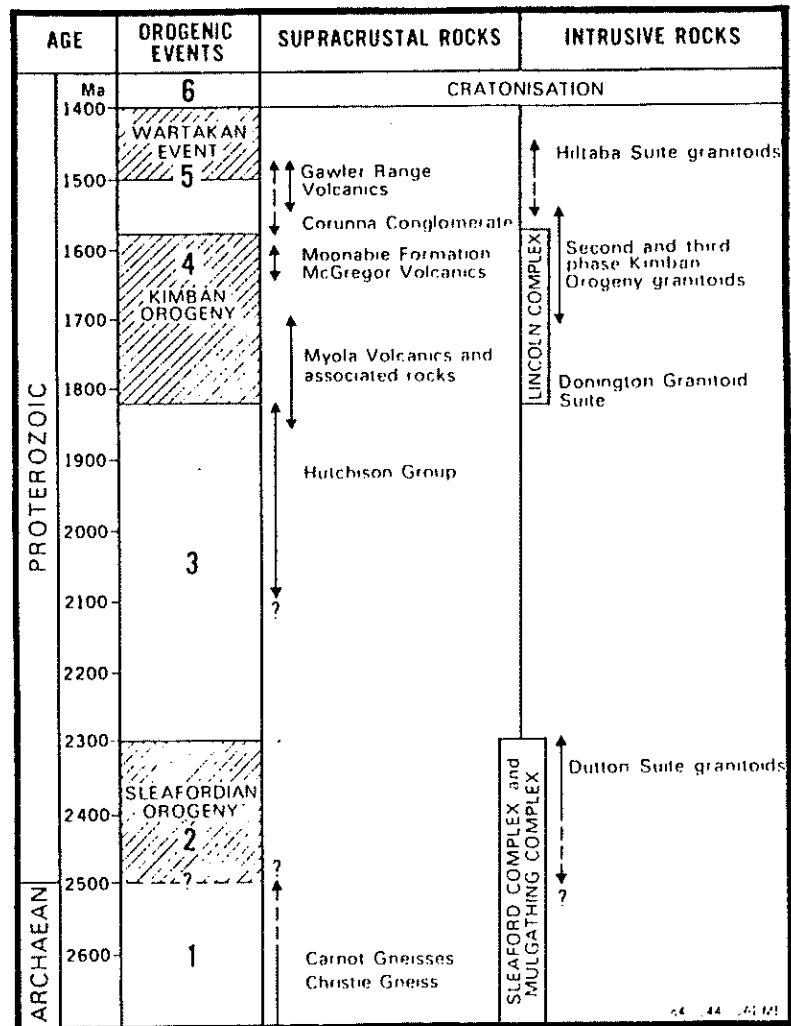
FIGURE 2   Summary of chronological and stratigraphic

subdivisions of Precambrian sequences in the Gawler Craton.

(from Webb et al.,1986)

CHAPTER 3 KOKATHA REGION - NORTHERN GAWLER RANGE VOLCANICS

3.1 PREVIOUS INVESTIGATIONS

The Kokatha area has been studied by both Blissett (1975) and Branch (1978). Blissett considers the area to be a series of volcanic units stacked in an easterly dipping sequence (the Chitanilga Volcanic Complex) overlain by the more voluminous Chandabooka Dacite. Branch, however, interpreted the volcanic succession to be somewhat more complex. He suggested the area was a caldera type structure with four phases of volcanic activity being recognized (Stratovolcano Phase; Premonitory Caldera Phase; Caldera Phase; and Post Caldera Phase; see fig.3).

Evidence for Branch's caldera is somewhat scant. The air photo pattern shows the main ignimbrite sheet in the eastern half of Kokatha is contained in a saucer shaped structure 15 Km long and 10 Km wide which resembles a typical caldera in shape and size (Branch,1978). The western margin of this structure he suggests coincides with a fault which displaces the volcanic pile.

Branch (1978) interpreted four phases of volcanic activity which he based on a sequence of volcanic phases similar to those proposed by Lipman (1975) for the Platoro Caldera in the San Juan ash-flow province of south-western United States.

The Stratovolcano Phase, being the first phase, consists of a basalt-rhyolite bimodal unit. Branch (1978) described this unit as thick piles of tholeiitic basalt, potassic basaltic andesite and minor dacite to rhyolite. This unit, he suggested, outcroped in two areas: Furthest west of the volcanic pile and east of the Kingoonya-Kokatha road. These two outcrops were interpreted to be the same, repeated by faulting, by correlating unusual potassic basaltic andesite flows in both sequences.

8

3.2 LITHOLOGICAL DESCRIPTIONS

3.2.1 BASALTS

Basalts occur in two areas of the mapped region (fig.3b & 4). Furthest to the west a thick succession of basalt flows are interbedded with thin dacite ignimbrite layers and rhyolitic air fall tuffs. At the base of the predominantly basaltic units a dacite unit is present representing the oldest exposed rock unit of the volcanic pile. The basalt is mostly characterized by poor outcrop however some well preserved flows are present, showing an increase in vesicles towards the top of the flow unit. In most instances the vesicles have been filled to form quartz amygdales (plate 1.1).

The other basaltic unit within the pile outcrops on the western side of the ridge east of the Kingoonya-Kokatha road. The outcrop is mostly highly weathered with little evidence for individual flow units. Above the basalt, rhyolitic units are present suggesting bimodal volcanism, as was evident with the basalt units furthest west in the mapped area.

3.2.2 ANDESITE

Andesites outcrop stratigraphically above the basalt layer and thin rhyolitic unit on the western ridge east of the Kingoonya-Kokatha road (fig.3b & 4). They characteristically form a prominant outcrop of fresh looking, grey groundmass, pink phenocrystic rock. Towards the east the andesites appear to increase in phenocrystic content.

3.2.3 DACITE-RHYODACITE

Dacitic to rhyodacitic lavas outcrop over a large area of the

9

map.   A   thick unit outcrops immediately above the western basalts
and is characterised as a compound unit of two distinct rhyodacites.
One   has   a typical black groundmass with pink to creamish coloured
phenocrysts.   Flowbanding   often   is evident with fine red-brown
groundmass   material   interlayered   with   thicker   dark   groundmass
dacitic layers (possibly suggesting magma mixing).   The other   unit
has   a   red-brown   groundmass   with   pink   coloured   phenocrysts   of
feldspar and less evidence for flowbanding.   Generally the units dip
20   degrees   to the east however locally contorted flows are   common
(plate   1.2).   These contortions possibly reflect   original   rugged
volcanic topography.   Rare brecciation of the flow banded rhyodacite
(plate 1.3) indicate possible autobrecciation during cooling of the
lava.

        Overlying this compound unit is another rhyodacite.   They are
separated by a band of thin rhyolitic tuffs.   The rhyodacite looks
similar to the previous one however it is distinguished by a darker
brown   to grey groundmass and altered pink phenocrysts   with
flowbanding being more prevalent.

        Dacites   outcrop   further   to   the   east   where   both   a   grey
groundmass   dacite and the Chandabooka Dacite are   present   (fig.4).
The Chandabooka Dacite is essentially a monotonous unit of red-brown
to   dark   grey groundmass and creamish coloured   phenocrysts.   The
outcrop   varies   from highly weathered to some fresh areas   where   a
rounded   weathering   pattern   is   evident.   Little   evidence   of
flow banding exists in this dacite suggesting a pyroclastic origin.

        The   grey   groundmass dacite outcrops in a thin band   above   a
thick   rhyolitic   unit   which thickens considerably in   a   southward
direction.   Large   pink   feldspar   phenocrysts   (up   to   1   cm)
distinguish this dacite from other dacites.

3.2.4 RHYOLITES

Both east and west of the Kingoonya-Kokatha road a series of rhyolitic ignimbrites, air-fall tuffs, flow breccias, pyroclastic and epiclastic layers outcrop (fig.4). The rhyolite ignimbrites are easily recognised in the field due to abundant quartz phenocrysts up to 2 mm in diameter. Larger phenocrysts of white and pink feldspars up to 4mm in diameter are present as are abundant xenoliths of more mafic looking material. The rhyolite ignimbrites dip approximately 20 degrees to the east and are mapped into three units due to slight changes in appearance.

Overlying the rhyolite ignimbrites an oval shaped rhyolitic breccia flow outcrops. Large dark groundmass xenolithic material (up to 50 cm in size) are included in a lighter groundmass flow banded rhyolite (plate 1.4). The shape of the outcrop possibly reflects some type of palaeotopographic valley infill from some nearby vent.

Above the rhyolite ignimbrites and rhyolitic breccia flow lie a series of thin rhyolitic flowbanded layers, accretionary lapilli, airfall tuffs, brecciated rhyodacites with sinter epithermal quartz, pyroclastics and reworked, epiclastic sedimentary units. This series of units probably represent a period of relatively low volcanic activity with respect to volumes of material ejected. Accretionary lapilli (plate 1.5) and thin tuff units are indicative of explosive volcanic activity (Cas & Wright,1987). The presence of epiclastics indicates reworking of the volcanic pile in quiescent periods. Epithermal quartz (plate 1.6) suggests that hydrothermal circulation systems were able to be established allowing the mobilization of minerals in heated meteoric waters. Hydrothermal systems may have not been generated at other times due to the dominance of voluminous, high temperature volcanic activity, preventing any hydrothermal circulation systems from becoming

established. Rhyodacitic breccias in which the epithermal quartz is hosted (plate 1.6) may be evidence of faulting with hydrothermal circulation systems often depositing their minerals in zones of weakness such as along fault zones. The brecciation may, however be formed by volcanic means with autobrecciation of a moving solid lava flow.

3.3 DISCUSSION

Ground evidence from my mapping suggests little conclusive evidence for Branches caldera structure and four phases of activity. Two cycles of volcanic activity looks more likely with a cycle consisting of initial basalts and some dacitic and rhyolitic units (units BW and BE to AE; see fig.3b). This is then followed by voluminous rhyodacites and dacites with some thin rhyolitic tuffs and pyroclastics (RD1 to RD2 and RH4 to D1). Rhyolitic ignimbrites, airfall tuffs, rhyolitic flows, epiclastics and pyroclastics are the final phase in the volcanic cycle (RH1 to VL-2). This last phase of activity is not seen in cycle 2.

The style of volcanism at Kokatha however is consistant with subaerial stratovolcano sequences as Branch (1978) has suggested.

3.4 MODERN EXAMPLES

Modern examples similar to the type of volcanism seen at Kokatha occur in the Cainozoic Basin and Range province of the southwestern United States. The combination of large scale extension, volcanism and sedimentation characterise the province (Gans et al.,1989). Lipman, (1984) has summerised features of well studied calderas and ash flow volcanic fields in western North America. Common rock types are series of ash falls, lava flows and voluminous dacitic to rhyolitic ignimbrites. Examples of voluminous

ignimbrites being the Kalamazoo Tuff (Gans et al.,1989), the Fish Canyon Tuff (Whitney & Stormer,1984) and the Bishop Tuff (Hildreth,1979).

FIGURE 3   Stratigraphic comparison of rock relations in the
            Kokatha region, between Branch (1978; 3a) and
            Robertson (1989; 3b)

FIGURE 3

a BRANCH 1978

CAINOZOIC

CAINOZOIC SEDIMENTS

MIDDLE PROTEROZOIC INTRUSIVE PHASE

HILTABA GRANITE

POST CALDERA PHASE
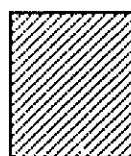
RHYOLITE DYKES

RHYOLITE BRECCIA PIPE

RHYOLITE-RHYODACITE IGNIMBRITE UNIT
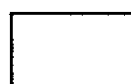
RHYOLITE DOME UNIT

CALDERA PHASE

CHANDABOOKA DACITE CALDERA & OUTFLOW FACIES
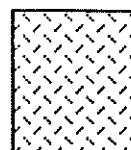
PREMONITORY CALDERA PHASE

DACITE-RHYOLITE UNIT
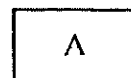
RHYOLITE-RHYODACITE DOME & FLOW UNIT

ANDESITE-RHYODACITE UNIT

STATOVOLCANO PHASE

BASALT-RHYOLITE BIMODAL UNIT

ARCHEAN

GNEISSIC GRANITE

b ROBERTSON 1989

CAINOZOIC

CAINOZOIC SEDIMENTS

MIDDLE PROTEROZOIC

HILTABA GRANITE

CYCLE 2

CHANDABOOKA DACITE D1

VOLCANICLASTIC VL5

RHYOLITE RH5

DACITE TBD

DACITE GMD

VOLCANICLASTIC VL4

RHYOLITE-RHYODACITE UNIT RH4

ANDESITE AE

FLOW BANDED RHYOLITE FRH

BASALT BE

CYCLE 1

EPICLASTIC VL2

EPICLASTIC TU4

RHYODACITE RU1

VOLCANICLASTIC VL1

AIR FALL TUFF TU3

FLOW BANDED RHYODACITE FR1

RHYODACITE BGD

RHYOLITE BRECCIA FLOW BF

RHYOLITIC IGNIMBRITE UNITS RH1, RH2 & RH3
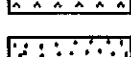
AIR FALL TUFF TU2

RHYODACITE UNIT RD2

AIR FALL TUFF TU1

RHYODACITE UNIT RD1

BASALT BW

RHYODACITE BW2

BASALT BW

DACITE BW

BASALT BW (with rhyolitic tuffs)

RHYODACITE BW1

PLATE 1.1   Vesicular basalt flow unit. The vesicles have
            been filled to form quartz amygdales.

PLATE 1.2   Weathered surface of a rhyodacite showing
            typical contorted flow banding.

PLATE 1.3   Rhyodacite breccia suggesting autobrecciation of
            a cooling lava.

PLATE 1.4   Rhyolitic breccia flow showing xenolithic
            dacitic material within a viscous rhyolitic
            melt.

PLATE 1.5   Photomicrograph of a portion of an accretionary
            lapilli.

PLATE 1.6   Epithermal sinter quartz within a rhyodacitic
            breccia

1.1

1.2

1.3

1.4

1.5
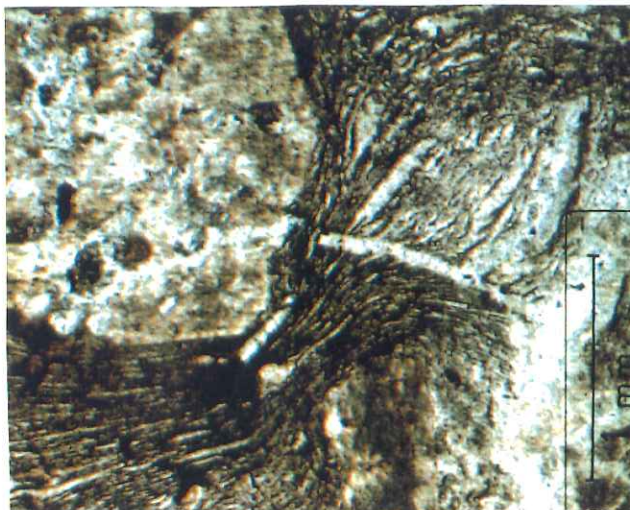
1.6

CHAPTER 4 PETROGRAPHY

4.1 INTRODUCTION

The following chapter aims to give a summary of important aspects of the petrography and mineralogy of the main lithology types seen at Kokatha. Sample locations and brief thin section descriptions are given in appendix 1. Mineral compositions used in this chapter were determined by electron microprobe analysis. For more detailed microprobe results see appendix 2.

4.2 BASALTS

Basalts in the area are mostly quite weathered, however fresh outcrops of basalt flows occur both in vesicular (amygdaloidal) and non-vesicular form. The basalts are fine grained, consisting mostly of plagioclase and clinopyroxene with ilmenite and magnetite (see plate 2.1).

Plagioclase is in the range oligoclase to labrodorite Ab45-Ab78 (fig.5), with most in the andesine to labradorite range. They occur as elongate grains of up to .5mm in size. Twinning is fairly poor however Carlsbad twinning can be seen on some grains. Plate 2.1 shows aligned plagioclase crystals indicating flow of the basalt lava.

Pyroxene mineral data indicate two distinct groups of basalts (fig.7). Basalts lower in the volcanic pile (eg. sample 908-123) have only Mg rich augite ($Ca_{28}Mg_{60}Fe_{12}$) as the only pyroxene composition. Basalts higher in the volcanic pile (eg. sample 908-150) has 3 pyroxene compositions, augite (av. $Ca_{39}Mg_{40}Fe_{21}$), ferroaugite ($Ca_{27}Mg_{31}Fe_{42}$) and pigeonite ($Ca_{8}Mg_{41}Fe_{51}$ to $Ca_{14}Mg_{42}Fe_{44}$). Larger grains show a subhedral shape with typical augite birefringence. Smaller grains have generally been altered

14

mostly to chlorite.

Oxides have been identified as ilmenite and magnetite for the lower basalt and titanomagnetite, ilmenite and magnetite for the higher basalt with accessory minerals of epidote, sphene and zircon being common in both.

A feature of all basalts is the the absence of olivine.

4.3 ANDESITES

Andesite in the field was characterized by a fine grained groundmass with large pink feldspar phenocrysts (up to 5mm). In thin section the feldspar phenocrysts are highly altered with no multiple twinning and only rare Carlsbad twinning. Microprobe analysis for sample 908-146 indicates almost all feldspar are alkaline (fig.5). Exsolution in the alkaline feldspars has completely unmixed the two end members making the initial composition hard to retrieve. Feldspars in the groundmass of the andesite appear highly altered making identification difficult.

Pyroxenes present in the andesite include augite (av. $Ca_{40}Mg_{39}Fe_{21}$), ferroaugite $(Ca_{28}Mg_{30}Fe_{42})$ and pigeonite $(Ca_{13}Mg_{37}Fe_{50})$, compositions that are similar to the higher basalts (fig.7). They are generally subhedral in shape occurring often as an agglomeration of grains. Pigeonite is present in some pyroxenes as cores with ferroaugite compositions at the rim. Clinopyroxene in the groundmass has mostly been altered.

Hornblende is present as large crystals showing characteristic 120 degree angles and pleochroism. However alteration to chlorite occurs on most grains with smaller grains being totally consumed.

Accessory minerals include epidote and sphene with opaques of magnetite and titanomagnetite.

4.4 DACITE/RHYODACITE

Dacite/rhyodacites in thin section are characterized by a high degree of devitrification of groundmass. This results in a microcrystalline, granular groundmass of mostly quartz and alkali feldspar. In some rhyodacites this devitrification gives rise to a perlitic texture as seen in plate 2.2. Flowbanding can be seen on the microscopic scale where viscous rhyolitic flow can be seen within the ignimbrite.

Phenocrysts within the dacite/rhyodacites (plate 2.3) consist of both plagioclase and alkali feldspar. Microprobe analysis for the three rhyodacites shown, indicate the feldspars are mostly altered with plagioclase of albite composition and alkali feldspars of perthitic microcline (fig.6).

4.5 RHYOLITES

Rhyolitic ignimbrites consist of a high number of quartz (crystalline and polycrystalline) and alkali feldspars. Xenoliths of more mafic material are present however under thin section these are highly altered and difficult to determine. The groundmass is generally devitrified however remnants of possible welded pumice fragments can be seen (plate 2.4). Quartz and feldspar grains are angular in shape and generally unwelded. Texture of the rock and xenolithic fragments possibly incorporated during eruption indicates explosive volcanic activity.

The mineralogy of the rhyolitic breccia flow is similar to the rhyolitic ignimbrites, however phenocrysts of quartz and alkali feldspar are more abundant as are xenolithic fragments. Some rhyolitic flow banding can be seen and welding of grains is moderate indicating a higher eruption temperature than the rhyolitic ignimbrites. Numerous angular xenolithic fragments indicate

16

explosive volcanic activity.

Rhyolitic air fall tuffs consist of angular fine grained quartz and alkali feldspar. Their mineralogy is generally not well preserved however some lamination is present indicating some sorting of grains during deposition.

Epithermal quartz occurring with rhyodacitic breccias displays a typical vein growth texture (plate 2.5).

Rhyolite to rhyodacite flow banded rocks of unit RH4 have a similar mineralogy to the dacite/rhyodacites previously discussed. The groundmass is devitrified consisting mostly of quartz. Phenocrysts are generally less abundant than in the dacite/rhyodacites, consisting of albite and K-feldspar. Doleritic xenoliths also occur in the unit (plate 2.6).

4.6 EPICLASTIC SEDIMENTS

Epiclastic sediments are of two types. Sample 908-39 is a grey to dark grey banded series of upwardly fining beds of mostly quartz grains in an aphantic matrix. Grains vary from approximately .3mm in diameter fining up to about .01mm in diameter. These upwardly fining beds possibly represent lake sediments laid down in a quiescent period.

A coarser sediment can be recognized (sample 908-40). The grains are subangular in texture consisting of quartz, feldspar and rock fragments of up to 5mm in size. The rock fragments have been altered somewhat making determination difficult. The matrix is generally fine grained quartz.

PHOTOMICROGRAPHS

PLATE 2.1   Basalt showing aligned, elongate plagioclase grains indicating flow. Smaller Clinopyroxene grains and oxides, ilmenite and titanomagnetite make up the other constituents of the mineral assemblage.

PLATE 2.2   Perlitic texture formed by the devitrification of glassy material, seen here in a groundmass of a rhyodacitic sample. (Width of view = 3.5 cm).

PLATE 2.3   Rhyodacite showing an agglomeration of both plagioclase and K-feldspar The groundmass consists of devitrified glass of mostly quartz and K-feldspar

PLATE 2.4   Rhyolitic ignimbrite consisting of quartz grains (crystalline and polycrystalline), albite and altered K-feldspar.

PLATE 2.5   Epithermal sinter quartz displaying typical vein growth texture.

PLATE 2.6   Dolerite xenolith within rhyodacite with altered K-feldspar and plagioclase phenocrysts. The groundmass is mostly composed of quartz and K-feldspar.

2.1
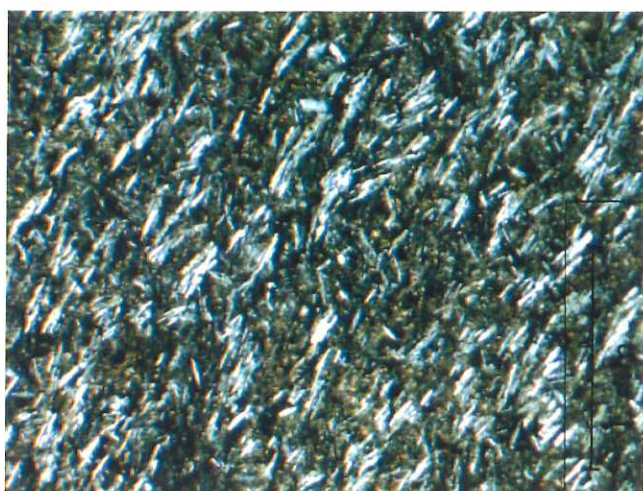
2.2
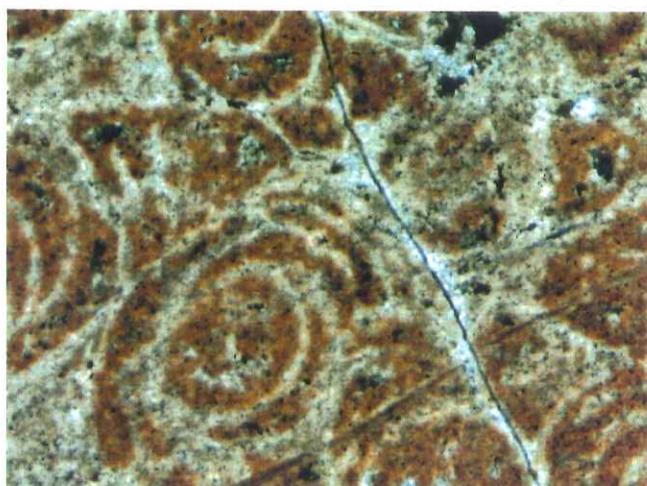
2.3

2.4

2.5

2.6
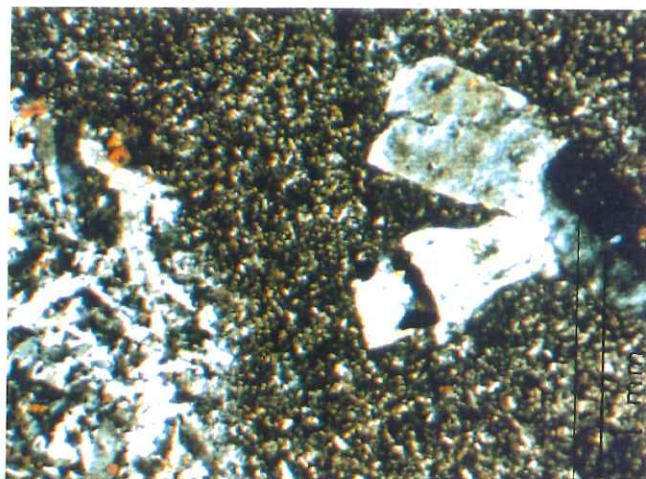
FIGURES 5 & 6   Anorthite - Albite - Orthoclase ternary

diagram showing feldspar compositions for

analysed samples.

FIGURE 7   Wollastonite - Enstatite - Ferrosilite

ternary diagram showing pyroxene composition

for analysed samples.

KEY (figures 5,6 & 7)

◼   Rhyolite RH1   (908-44)

 o   Rhyodacite RD1   (908-111)

+   Rhyodacite BW   (908-122)

Δ   Basalt BW (Mg rich; 908-123)

◆   Rhyodacite RD1   (908-137)

□   Andesite AE   (908-146)

●   Basalt BW (Mg poorer; 908-150)

FIGURE 5

FIGURE 6

FIGURE 7
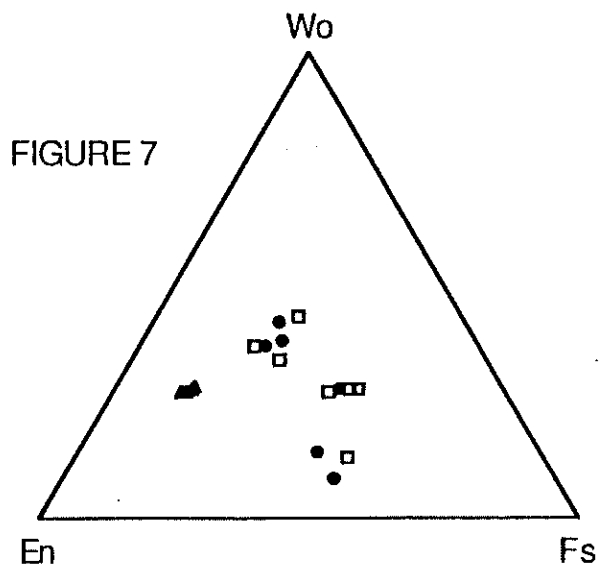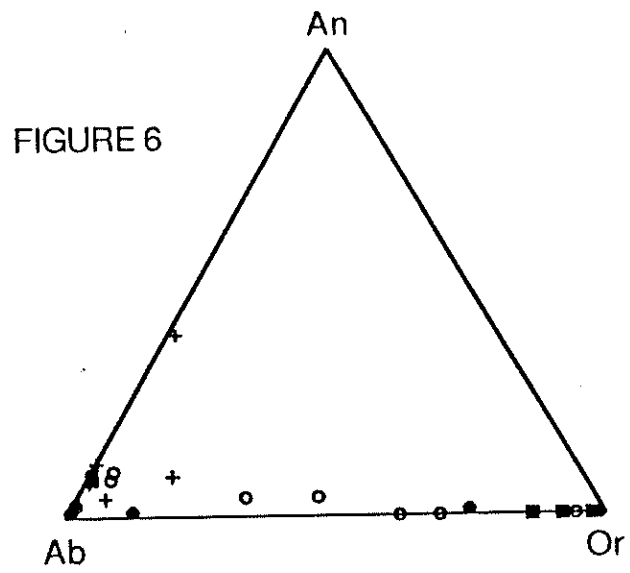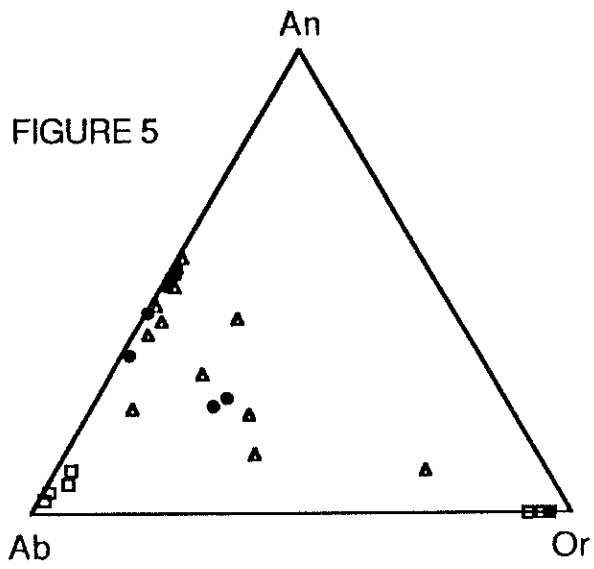
CHAPTER 5 GEOCHEMISTRY

5.1 INTRODUCTION

The following chapter discusses the major and trace element chemistry of the Kokatha volcanics and other comparable volcanic provinces. Whole rock analysis of samples from Kokatha can be found in detail in appendix 3 along with a sample location map.

Generally Lowder's (1972b,1973a; fig.8) classification for rocktypes in the Gawler Range Volcanics has been followed. It should be noted sample 908-120 has been plotted as a basalt even though Lowder's scheme classifies it as an andesite. This has been done due to this rocks association with basalt rocks in the western part of the mapped area.

5.2 MAJOR AND TRACE ELEMENTS

5.2.1 MAJOR ELEMENTS

All major elements show reasonably expected trends when plotted against SiO_2 (figs.9 &10). A point of interest is the relatively high alkaline concentrations which is a feature of the Gawler Range province as a whole (Giles,1988). Elements such as TiO_2, Fe_2O_3, MgO, CaO, Al_2O_3, MnO, and P_2O_5 all show trends of decreasing concentrations with increasing SiO_2. This behaviour along with K_2O and Na_2O enrichment with increasing SiO_2 is broadly comparable with the generation of magmatic diversity by fractional crystallization of relatively mafic parent magmas.

In all trends of depletion with respect to increasing SiO_2 a good curvi-linear relationship can be fitted from 58 to 78% SiO_2 (fig.9). This linear relationship breaks down in the basalt field with some very large variations of element concentrations occurring independantly of SiO_2 variation.

Na_2O and K_2O show considerable variability with respect to the concentration of major elements within the basalt, rhyodacite and rhyolite fields (figs.9 & 10). Some of the rhyolite and rhyodacite variation probably reflects alteration effects.

Significant overlaps in concentration ranges of elements (particularly in the basalt, rhyodacite and rhyolite fields; figs.9 & 10) is not consistent with a single continuous fractionation event.

5.2.2 TRACE ELEMENTS

Different minerals may incorporate or exclude trace elements with even greater selectivity than they do major elements (Cox et al.,1979). Because of this behaviour trace elements can give important information on the igneous processes which may have occurred in the system.

Trace elements have been plotted in a number of ways. Trace elements versus SiO_2 (figs 10 & 11) show a variety of trends. Elements such as Sr, Sc, Ni, V, Cu and Zn show a negative relationship in concentration with SiO_2. Rb, La, Th and Nd show positive correlations with SiO_2 variation. Zr, Ba, Y, and Ce all show an initial increase in concentration followed by a decrease in concentration between the rhyodacite and rhyolite fields when plotted against SiO_2. Hence trace element behaviour can be divided into three groups. (1) Those which are compatible with more mafic, high temperature minerals, (2) elements which are incompatible with those minerals (often referred to as Large Ion Lithophile (LIL) elements) and (3) those which are originally incompatible but become compatible with minerals in the dacite/rhyodacite field.

To analyse trace element behaviour, chondrite normalised incompatible elements have been plotted in approximate sequence of

increasing compatibility for a wide range of rocktypes (basalt to rhyolite; see fig.12).

Strontium, phosphorus and titanium show similar behaviour with enrichment in basalt and depletion in rhyolite (see also figures 9 & 10). Strontium displays an affinity with the feldspar group. In a fractionating system originating with basalt, strontium will become incorporated in plagioclase leaving the residual melt depleted in strontium. More silicic rocks derived from this residual melt, even though rich in feldspars, will be depleted in strontium compared to the basalt. Phosphorus and titanium are incorporated in the minerals apatite and ilmenite/titanomagnetite respectively, both early forming minerals present in mafic systems, so they too are depleted in rocks of rhyolitic composition.

Potassium, rubidium and thorium display a reverse relationship to phosphorus, strontium and titanium, being enriched in rocks of rhyolitic compositions. Potassium is a constituent in alkali feldspars and therefore has high concentrations in rocks such as rhyolites which have potassium feldspars. Rubidium is geochemically like potassium, so that it too is higher in concentration in rhyolitic rocks compared to basaltic rocks. Thorium shows an enrichment in more siliceous rocks reflecting its incompatibility to early formed (more mafic) minerals.

Other elements plotted in figure 12 do not show a straight forward concentration relationship with different rocktypes. Generally the concentrations of these elements in the basalt plotted (908-150) are not consistent with expected fractionation trends.

Barium when plotted against SiO_2 (fig.11) shows a general increase in concentration from basalt to dacite/rhyodacite fields followed by a decreasing trend in concentration towards rhyolitic compositions. This indicates barium becomes compatible (K_D >1) with

minerals forming from magmas of dacitic/rhyodacitic composition. At this time barium will become readily incorporated in potassium feldspar. Figure 12 indicates a much higher barium concentration for the basalt (908-150) than would be expected in a fractionating system. Plotting the normalised concentration of barium for a more Mg rich basalt (908-123), which lies closer to a fractionating trend line (see fig.11), does give the expected higher concentrations of barium in the dacite/rhyodacite field and lower concentrations in the rhyolite, andesite and basalt fields.

Samarium too, does not display a straight forward concentration relationship with different rocktypes. K_D values in general increase from La to Yb but often remain less than 1 (Nash & Crecraft, 1985). Sm would be expected to be more enriched in the dacite/rhyodacite and rhyolite than the basalt and andesite. The concentration of Sm in the basalt (908-150) is much higher than in the dacite/rhyodacite, rhyolite and andesite (fig.12), again indicating that this basalt is not a parent source for the more silica rich rocks.

Zirconium is different than most elements due to a combination of high charge and large ionic radius (Mason & Moore, 1982). It does not enter the common rock forming minerals to any degree but appears in a specific phase, zircon. Zirconium plotted against SiO_2 (fig.11) show a high concentration in the dacite and rhyodacite fields. This reflects the compatibility of zirconium in this field which is extracted from the melt to form zircon. Figure 12 indicates zirconium is more abundant in the dacite/rhyodacite and rhyolite than the andesite and basalt.

Rare earth elements (REE) have been investigated using Ce, Nd, Sm and Eu from the light rare earth elements (LREE) and yttrium representing the heavy rare earth elements (HREE). In general total

REE   increase in concentration from basalt to rhyolite.

Chondrite normalized REE have been plotted for a wide range of rocktypes (fig.13).   Increasing concentration of the REE occurs for andesite through to rhyolite.   The basalt plotted (9Ø8-15Ø) has a much higher concentration of REE than would be expected.   A more Mg rich basalt (9Ø8-123) has been plotted for Ce, Nd and Y giving a more expected series of increasing concentration of elements from the basalt to the rhyolite.   A negative europium anomaly exists in the dacite/rhyodacite rhyolite fields.   This reflects initial K-feldspar fractionation where Eu is readily incorporated into the crystal phase.

5.3 ELEMENT BEHAVIOUR WITH STRATIGRAPHIC HEIGHT

Given cyclism of observed volcanic stratigraphy and the possibility that these evolutionary cycles may be related to magma chamber dynamics, variance diagrams of major and trace elements against stratigraphic height were plotted.   Two cycles of volcanism appear to exist with a cycle as follows: Basalt - dacite - rhyodacite - rhyolitic ignimbrites, tuffs and volcaniclastics.   If fractionation is occurring to produce such a cycle, one would expect this to show up in element behaviour.

Two plots of stratigraphic height against elements are shown in figures 14 and 15 (Y and TiO_2 respectively).

From the height vs yttrium plot a case for fractionation cycles can be made.   Basalts evolving to rhyodacites appear to lie on some type of trend line with a spread of generally lower yttrium values for rhyolites at the top of the cycle.   The variance in yttrium values for the rhyolites possibly reflecting magma mixing and fractionation.   Dacite to rhyodacite at the top of the volcanic pile show a possible fractionation trend. Yttrium concentrations for

dacite and rhyodacite are lower than those in the first cycle indicating yttrium depletion.

Concentration of yttrium with stratigraphic height also indicates evolutionary cycles. Dacites and rhyodacites of cycle 1 have higher concentrations of yttrium when compared to dacites and rhyodacites of cycle 2. This suggests the second cycle originates from a source with lower concentrations of yttrium, possibly the result of remelting some refractory component of the first evolutionary cycle.

Incompatible elements (Y, Rb & Ce) vs SiO_2 variation diagrams (fig.10 & 11) also show a trend of lower concentrations in the second cycle.

The TiO_2 vs height diagram tells a slightly different story. Evolution of low TiO_2 (1%) to high TiO_2 (2.25%) concentration in the lower basalt unit suggests some type of fractionation trend. Fractionation trends also look likely for rhyodacite of units RD1 and RD2, and dacite to rhyodacite of units BMD and D1. Andesites possibly represent a mixing relationship between basaltic and rhyolitic magmas. Fractionation from basalt high in the western basaltic pile to a composition of overlying rhyodacites (RD1) looks unlikely.

can't follow on fig 15

5.4 BASALTS

As previously stated basalts in to the west of the mapped area have peculiarities in their element chemistry. Basalts low in the western basaltic pile (samples 908-72, 908-120 & 908-118) have a different element chemistry than basalts stratigraphically higher in this basaltic unit (samples 908-72, 908-150 & 908-21). The stratigraphically lower basalts are depleted in TiO_2, MnO, Fe_2O_3 and P_2O_5 when compared to the basalts higher in the unit (figures

10;11;14 & 15). MgO, however shows the reverse trend with its concentration being higher in the earlier formed basalts. CaO, Na$_2$O and K$_2$O do not seem to show any real relationship of this sort.

Modelling using a crystallizing magma package (igpet) has been used to determine if fractional crystallization can be responsible for the change in mineral chemistry between "lower" and "higher" basalts in the western part of the mapped region. The program models the compositional changes resulting from crystallization of a basaltic magma based on equations resembling those of Nathan and Kirk (1978). An initial composition in weight percent is entered with liquidus temperatures for a range of minerals being calculated. If the liquid is at or below the liquidus temperature of a mineral then a small percentage of that mineral is subtracted from the liquid. Hence the fractional crystallization of mineral phases is simulated.

Fractionation from a composition of sample 9Ø8-118 (low in the volcanic pile) has been attempted to generate mineral compositions crystallizing at given times (see table 1).

Plagioclase of composition An-Ab 71-68 initially crystallizes with Ca-poor pyroxene (En-Fs 85-85) and augite (Di-Hd 84-84) crystallizing after 3.7% crystallization. It is important to note olivine is not crystallized in this model as is the case from petrographic studies. Plagioclase has an initial crystallizing temperature of 1188.8°C with augite and Ca-poor pyroxene of 1177.9 and 1176.9°C respectively. Magnetite does not crystallize until 35.1% crystallization takes place at a temperature of 1137.2°.

From the tabulated data the residual melt of the parent basalt does not closely approximate the composition of the basalts higher in the volcanic pile. It seems unlikely that these basalt groups are related by fractionation processes alone.

Pyroxene geothermometry from microprobe data suggests higher temperatures. Pyroxenes from lower basalts are high in magnesium content. Using Lindsleys pyroxene geothermometry (1983) compositions suggest temperatures of $1300^{\circ}C$ (see fig. 16). Temperatures for pyroxene composition for the basalts higher in the volcanic pile indicate lower temperatures from 1050 to $1150^{\circ}C$. Similar temperatures for these pyroxene compositions are seen using diagrams constructed for higher pressures. This gives good evidence that the temperatures of the basalts were very hot with the two groups of basalts showing a temperature difference of some $200^{\circ}C$.

Mineral data (fig. 5) indicate pyroxenes from the lower basalts (sample 908-123) are much richer in magnesium than those in basalts higher in the pile reflecting the overall concentrations of major elements for these two magma groups. Higher temperatures of the basalts limit their ability to crystallize many phases. Such phases which are not likely to be crystallize at initial high temperatures are oxides such as ilmenite and magnetite and accessory minerals such as apatite.

Crystallization of Mg rich pyroxenes and plagioclase would deplete the melt in Mg and Ca, while increasing the abundance of Fe, Mn, K, and Na. Absence of crystalling oxides (magnetite and ilmenite) and apatite would tend to increase Fe, Ti and P concentrations in the melt (see table 1). Through crystallization of high temperature minerals a liquid of relatively lower Mg and Ca concentrations and higher Ti, Fe and P concentrations can be generated.

However, as previously stated, the increase in Ti and P cannot be attributed to fractionation processes alone. Large variation in concentrations of incompatible elements (figures 9,10 & 11) within and between the two groups of basalts are inexplicable on purely

25

fractional crystallization grounds.

5.5 EVOLUTION OF MAGMA COMPOSITIONS

Fractional crystallization has been investigated as a possible means for producing the apparent cycles seen at Kokatha. Two cycles are postulated, suggesting two fractionating magma bodies existed, a younger and an older.

Rb, Y and Ba plotted against SiO_2 show two possible fractionation trend lines and a possible mixing trend to produce the andesite (figs 10 & 11). The fractionation trend lines indicate a relative enriched (in incompatible elements Rb, Y & Ba) fractionation and a depleted fractionation trend. The enriched trend corresponds to the first observed cycle. The relatively depleted trend represents the rocks of cycle 2 where the source of the melt is possibly affected by refractory material from the evolution of the first cycle.

A mixing trend line can be drawn for the andesite representing a mixture of basaltic (Mg rich basalt) and dacitic to rhyolitic composition. The pyroxene mineralogy of the andesite is quite different from the pyroxenes in the Mg rich basalts (see fig.5). They are however remarkedly similar to pyroxene compositions found in Mg poorer basalts. Temperatures for the pyroxenes in the andesite are also similar to the Mg poor basalts giving temperatures of around 1150° C. Pigeonite cores and ferroaugite rims in some of the pyroxenes suggest mixing of magmas with non-complete re-equilibration of the pyroxene compositions.

Least squares mixing calculations have been performed between rocktypes of the area to see if they can be generated from each other. Generally fractionation from one composition to another has been carried out on samples which are not separated by large

differences in chemistry and have a close stratigraphic relationship. This has been done to reduce any errors brought about by using fixed compositions of crystallizing minerals. Mineral compositions used have been determined by microprobe analysis of type examples. Figures 14 and 15 show the relative stratigraphic positions of samples used.

The modelling system uses a bulk composition of liquid, crystallizes minerals of a known composition so as to produce a calculated daughter composition as close as that to the given daughter composition. How much of each mineral and their proportions are calculated leaving a percentage of melt of calculated daughter composition (see table 2). The residual squared value indicates the accuracy of the fractionation, the lower the value, the more accurate the fractionation.

The results from the fractionation program are tabulated in table 2. The residuals are generally high however the calculated daughter compositions do approximate the measured daughter composition. High residuals possibly suggest that mixing may be occurring between fractionated components.

Fractionating a magma of dacitic composition to produce rhyodacite and rhyolite appears very likely with reasonably low residuals being attained. Least squares mixing calculations indicates 25% crystallization of minerals, andesine, K-feldspar, augite and ilmenite (see Table 2) from a dacitic parent composition (sample 908-064) is needed to produce a rhyodacitic daughter composition (908-105). A further 33% crystallization of minerals, K-feldspar, albite, ilmenite and apatite from a melt of rhyodacitic composition (908-111) is needed to generate a rhyolitic daughter composition (908-001; see Table 2). Results from fractionation of basalts from the western pile are not satisfactory and suggest a

process other than fractional crystallization. Large variations in element chemistry indicate possible contamination from more crustal rocks.

Fractional crystallization with some mixing of fractionated components appears to be processes acting in the magma chambers to produce the variety of rocktypes seen at Kokatha. Some discrepancies are apparent indicating that other processes are also acting upon the system. Some mixing of fractionated components may tend to increase the Si content (for example) of the more mafic components to a higher level than by fractionation processes alone. Contamination from wallrocks is another possibility. This also would increase and decrease certain elements from that which could be expected from fractionation processes.

5.6 DISCRIMINATION DIAGRAMS

A series of discrimination diagrams have been described by a number of authors to distinguish between the various types of volcanic rocks.

Pearce and Cann (1973), plotted trace elements on ternary diagrams to determine tectonic setting of basic volcanic rocks. Figures 17 and 18 plot Zr, Ti/100 and Sr/2 and Zr, Ti/100 and Y*3 respectively. Both diagrams plot the basalts and andesites in the calc-alkaline field.

Miyashiro's diagram (1974;fig.19) distinguishes between tholeiitic and calc-alkaline basalts. The two groups of basalts are well illustrated, showing their differences in concentrations of Ti, Fe and Mg. The basalts plot near the calc-alkaline and tholeiitic boundary. Contamination from more crustal rocks as previously discussed may affect the outcome produced using these types of diagrams. The calc-alkaline nature of the basalts seen in these

rocks may be a reflection of contamination of a tholeiitic basalt source.

5.7 DISCUSSION

Geochemical data indicate both fractionation and mixing of fractionated components has produced the series of rock types seen at Kokatha. Two cycles are represented, with stratigraphic, geochemical and lithological evidence to support this assumption.

Basalts do not seem to act as a parent composition for more fractionated compositions (dacites, rhyodacites and rhyolites) suggesting some other source composition is needed but not represented in outcrop. High variability in element chemistry of the basalts may be due to high crustal contamination. This would allow all rock types seen at Kokatha to be derived from the same source. Fractionation, mixing of fractionated components and crustal contamination being the active magmatic processes in forming the variety of rock types seen at Kokatha.

Calc-alkaline volcanism is characterised by the abundance of rocks of andesitic composition occurring in plate subduction environments (Ehlers & Blatt, 1982). The general lack of rocks of andesitic composition over the whole Gawler Ranges (Glen et al.,1977; Giles,1988) suggests subduction processes are unlikely to have occurred.

Recent work in the Basin and Range province by Gans et al.(1989) suggest the high K calc-alkaline series were formed by synextensional volcanism. Similarities with the Gawler Range Volcanics include voluminous volcanic rocks of dacitic to rhyolitic compositions similar in size to the Yardea Dacite. Assimilation of intracratonic tholeiitic basalts with lower crustal rocks may occur. The tholeiitic nature of the basalts may

be lost due to assimilation with the lower crust hence compatibility diagrams plot the basalts within the calc-alkaline field.

FIGURES 9,10 & 11   Major and trace element variation diagrams.

Major elements expressed as weight %

trace elements in ppm.

KEY   (for figures 8-10)

+   Basalts

▢   Andesites

▮   Dacites

✗   Rhyodacites

O   Rhyolites

FIGURE 9
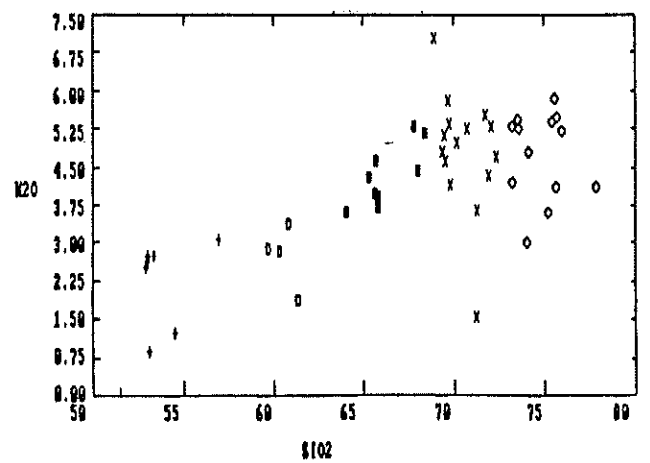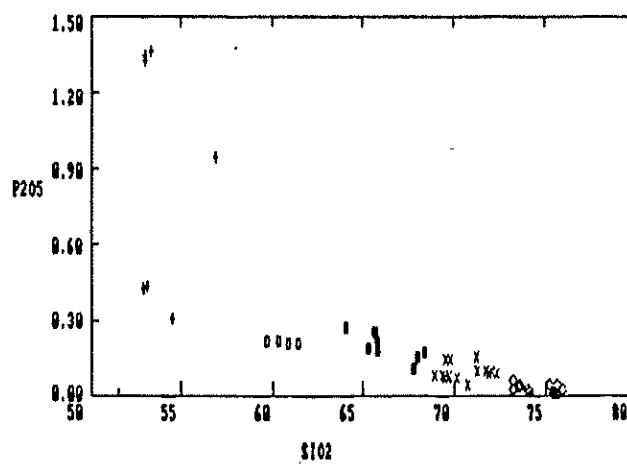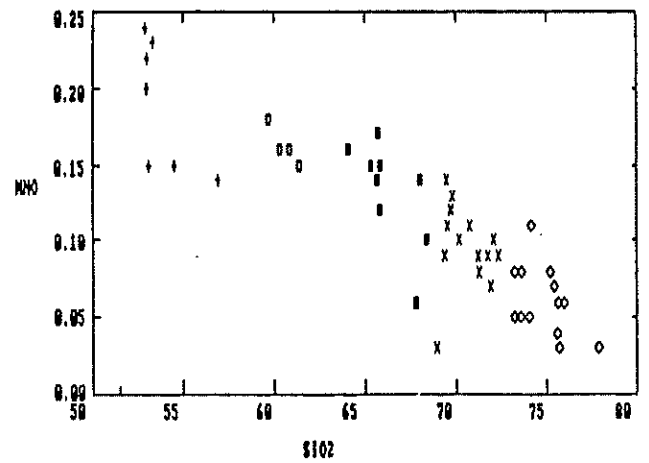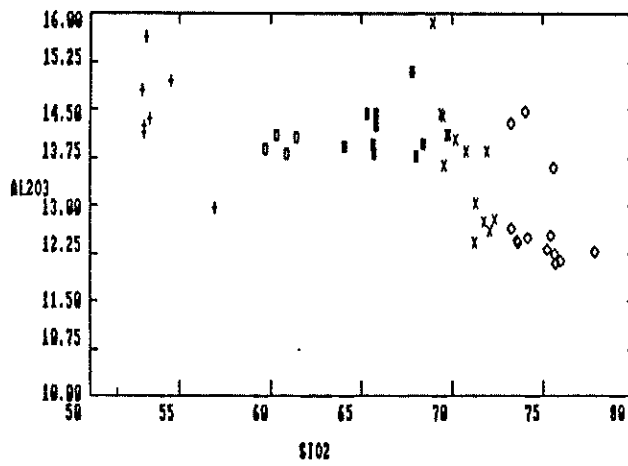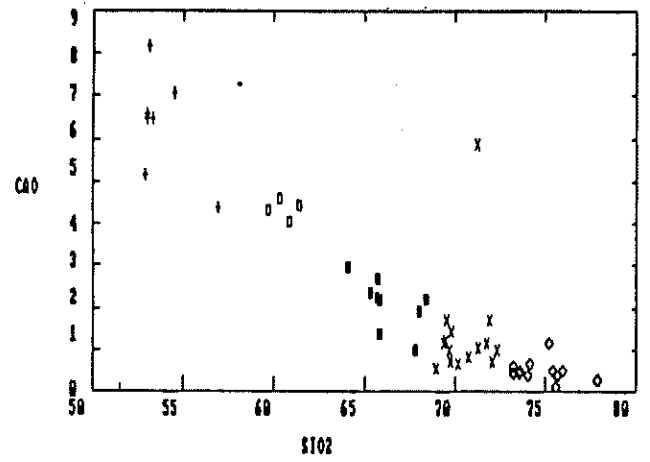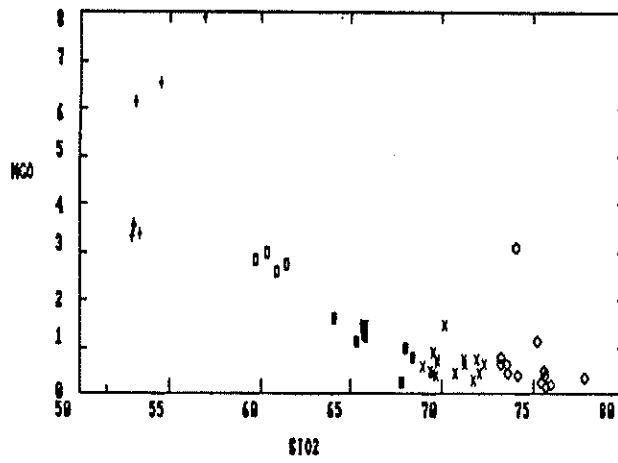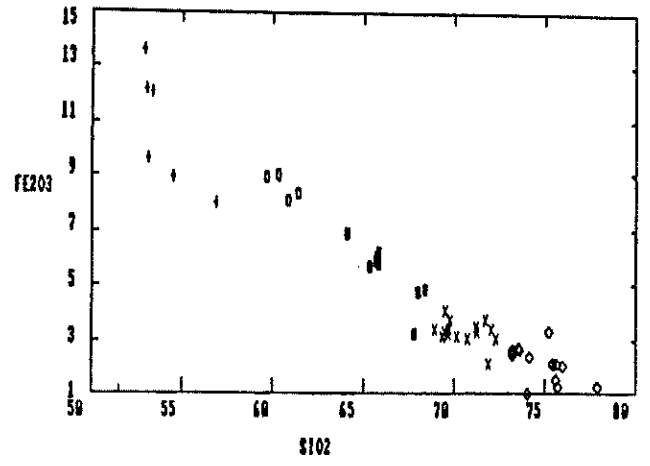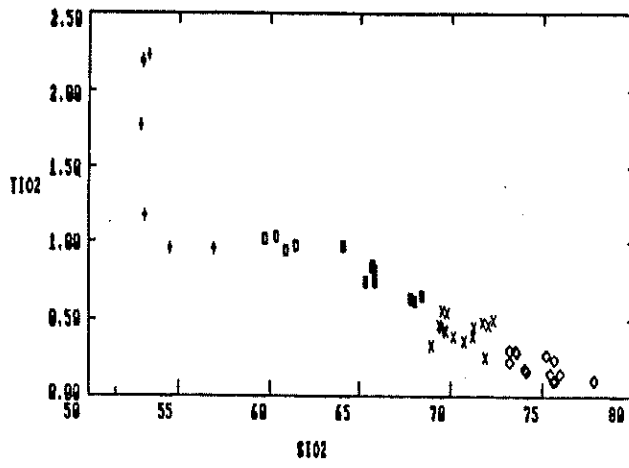
FIGURE 10
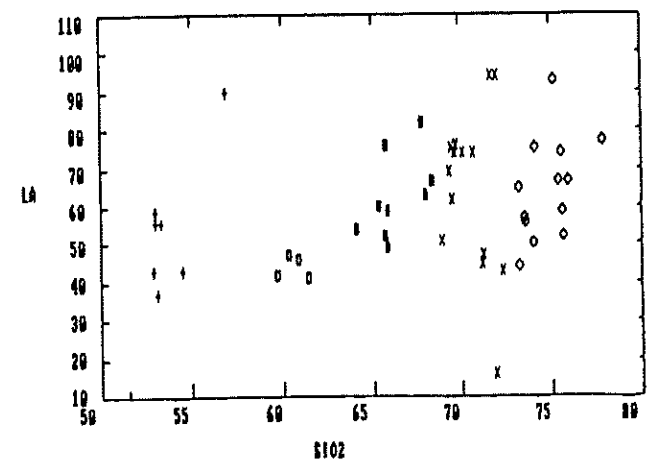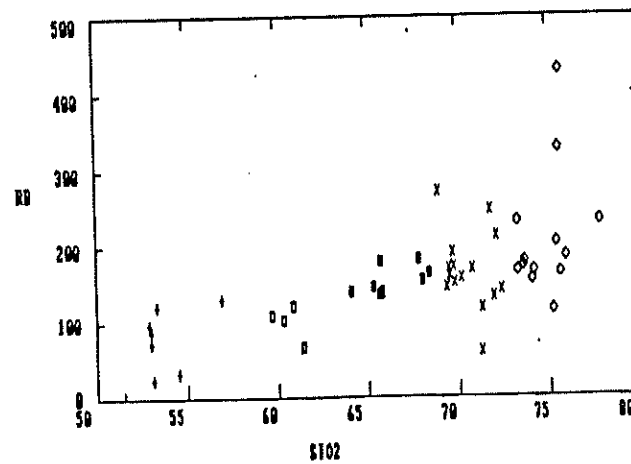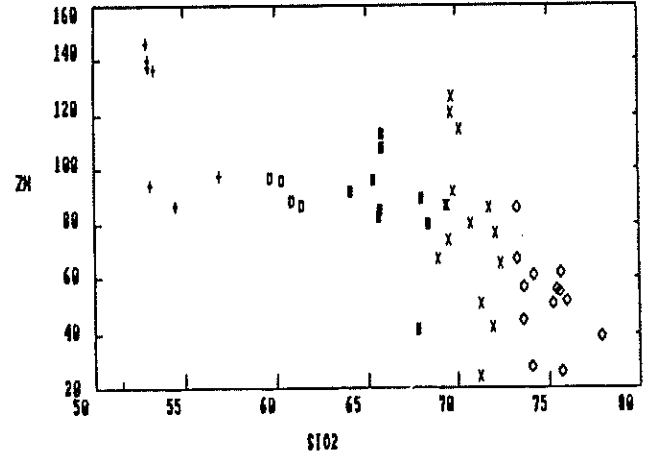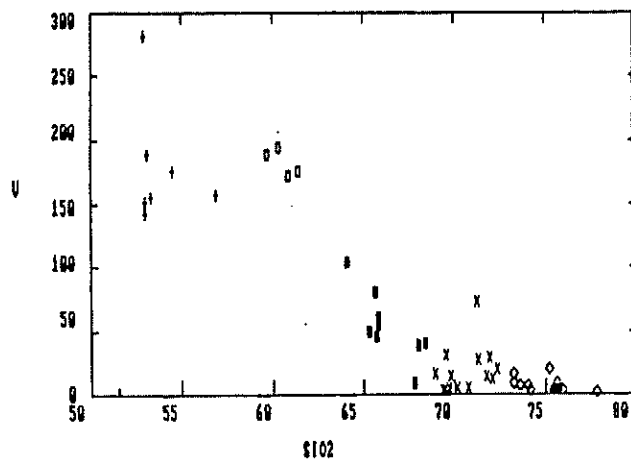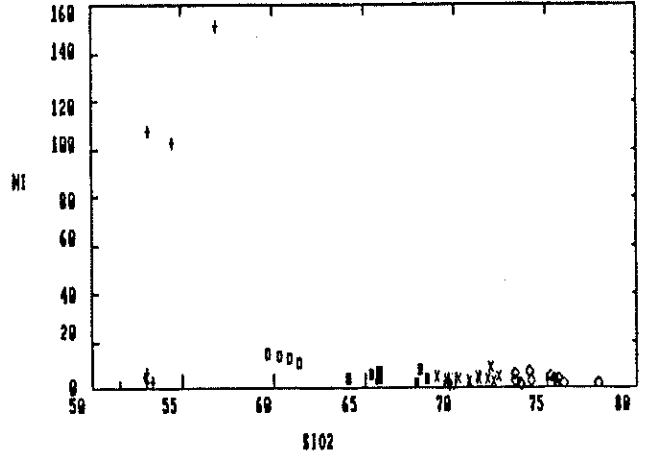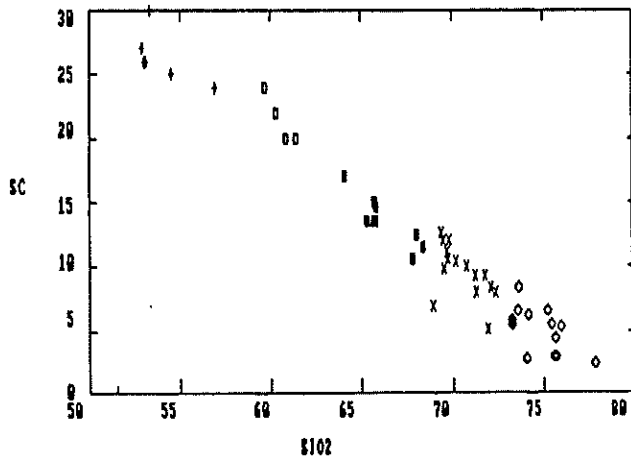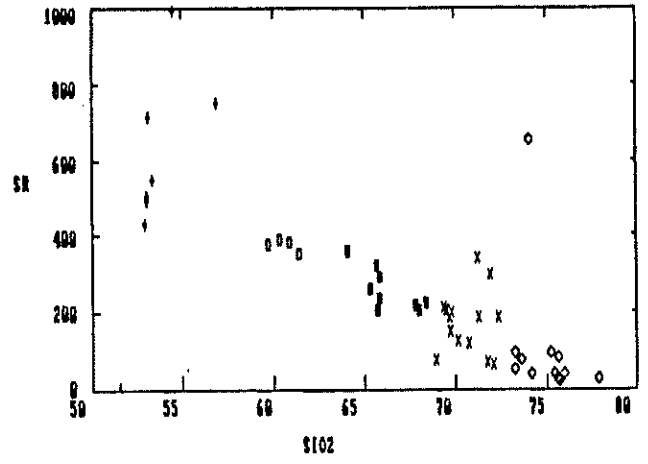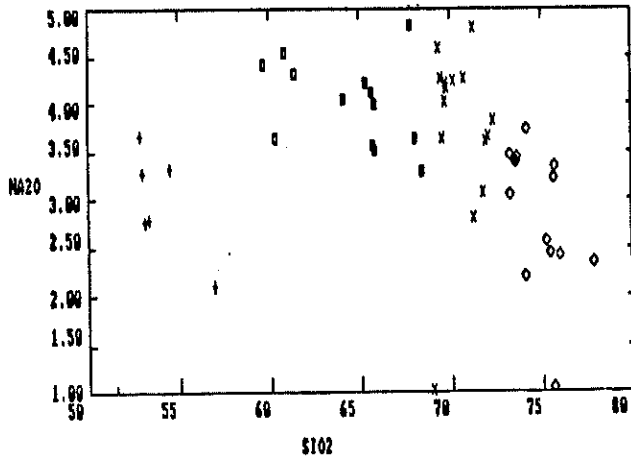
FIGURE 11
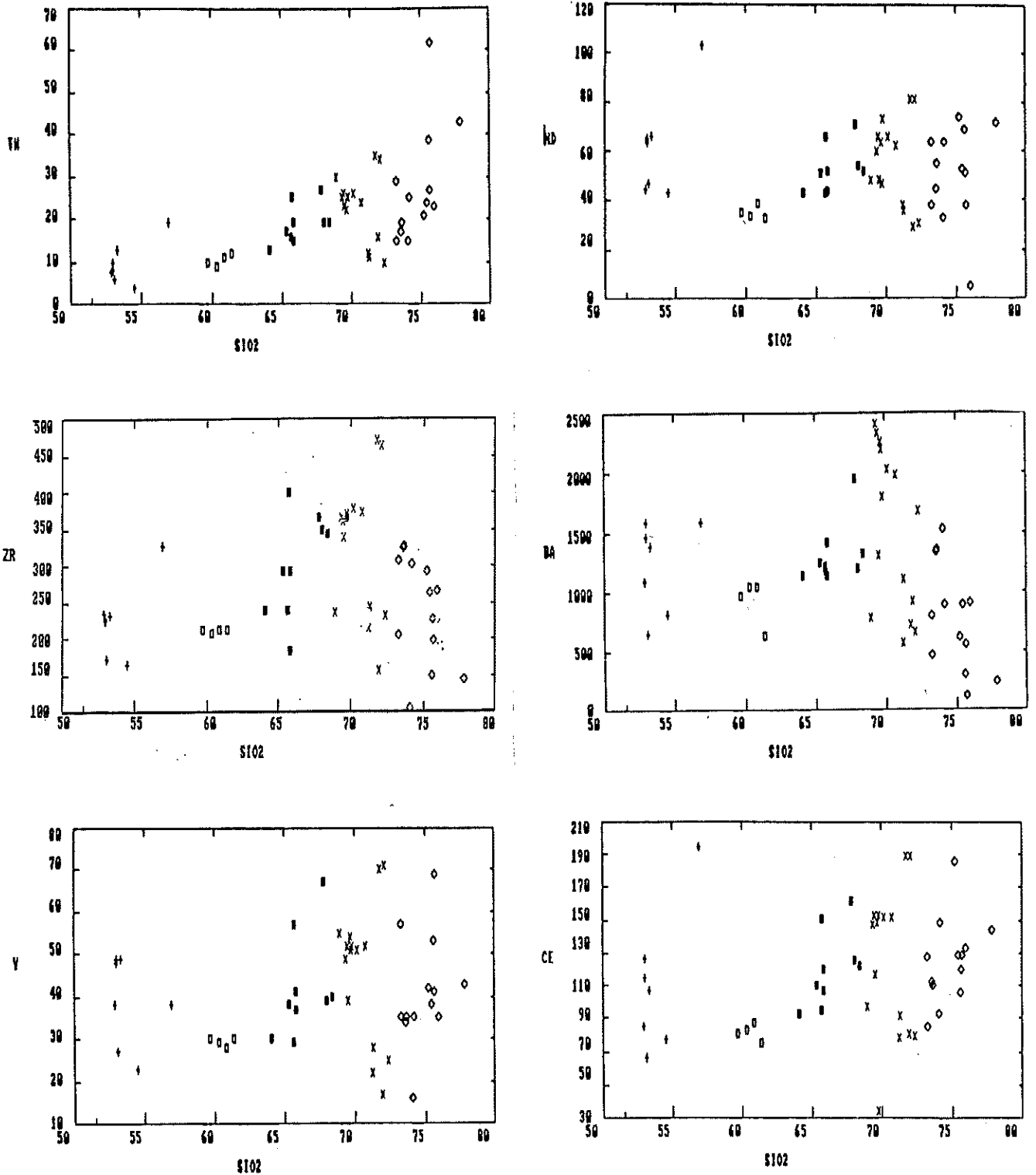
FIGURE 8
LOWDER
1972b, 1973a
% SiO2

BASALT	<55
ANDESITE	55-63
DACITE	63-69
RHYODACITE	69-74
RHYOLITE	>74

FIGURE 8   Rock classification for rocks in the Gawler Range

Volcanics, devised by Lowder (1972b;1973a).

FIGURE 12   A plot of incompatible element abundances,

normalised to chondrite for representative

samples from Kokatha.

KEY

━━   Rhyolite (908-001)

━━━   Dacite/rhyodacite (908-106)

━━━.   Andesite (908-18)

━━━.   Basalt (Mg poorer; 908-150)

FIGURE 12
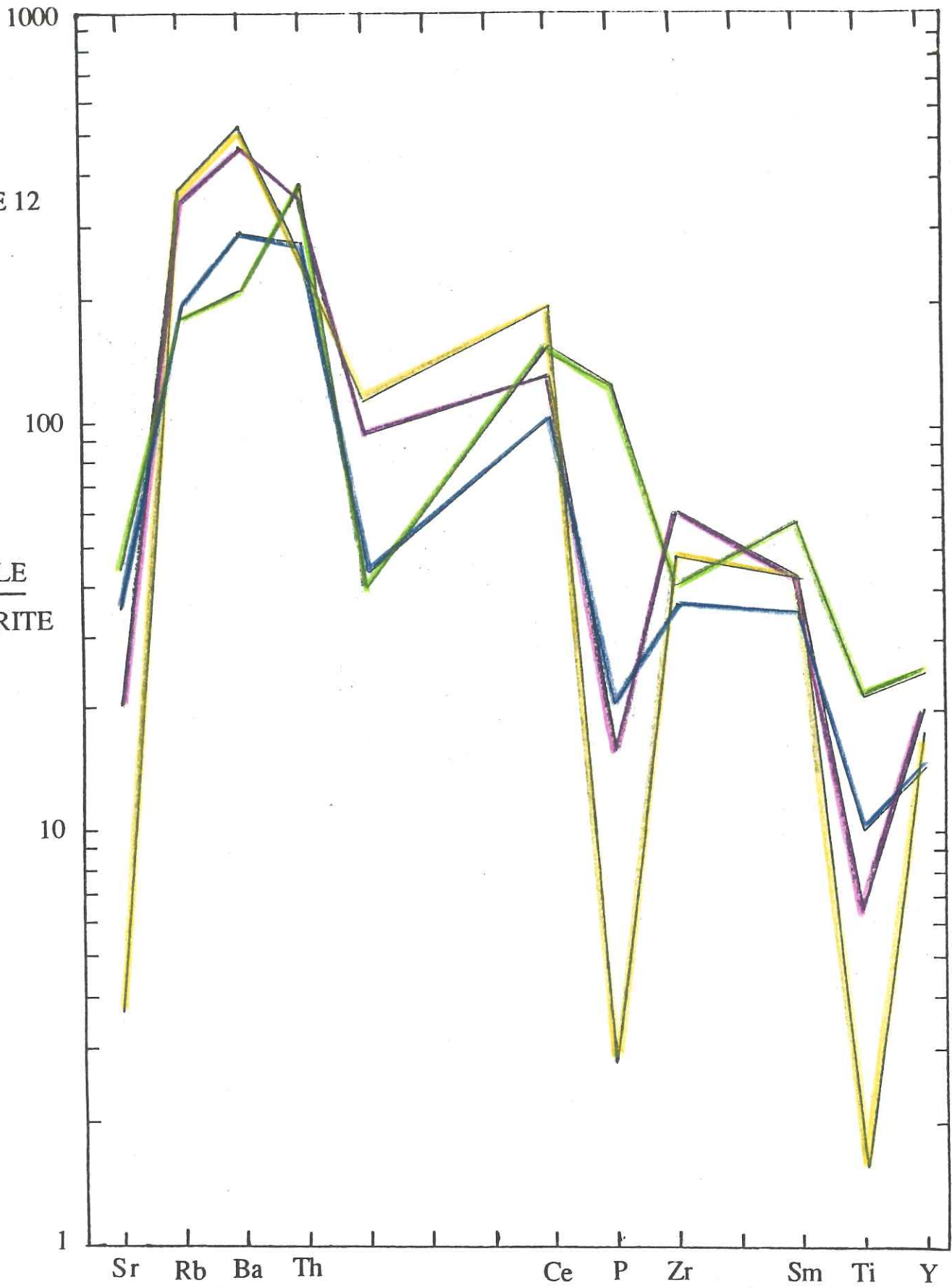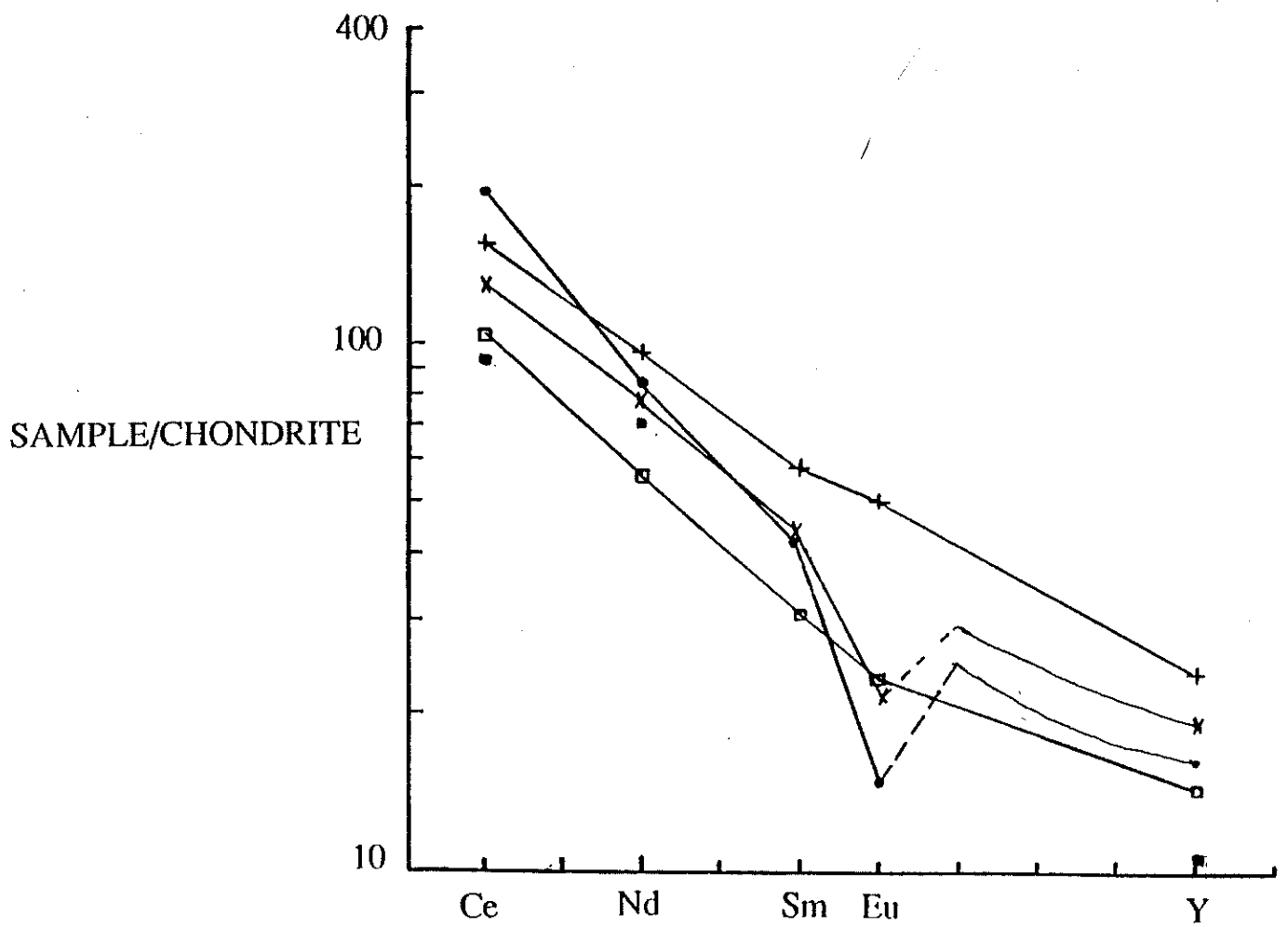
FIGURE 13   Plot of rare earth elements normalised to

chondrite for representative samples from

Kokatha.

KEY

•   Rhyolite (908-001)

✗   Dacite/rhyodacite (908-106)

◻   Andesite (908-18)

+   Basalt (Mg poorer; 908-150)

▮   Basalt (Mg rich; 908-123)

FIGURE 14   Element variation diagram plotting yttrium vs
             stratigraphic height.

FIGURE 15   Element variation diagram plotting TiO$_2$ vs
             stratigraphic height.

             KEY (figures 14 & 15)

             +   Basalts
             ⊓   Andesites
             ▇   Dacites
             X   Rhyodacites
             ⊙   Rhyolites

        Major elements expressed in weight % , trace
        elements in ppm.

FIGURE 14
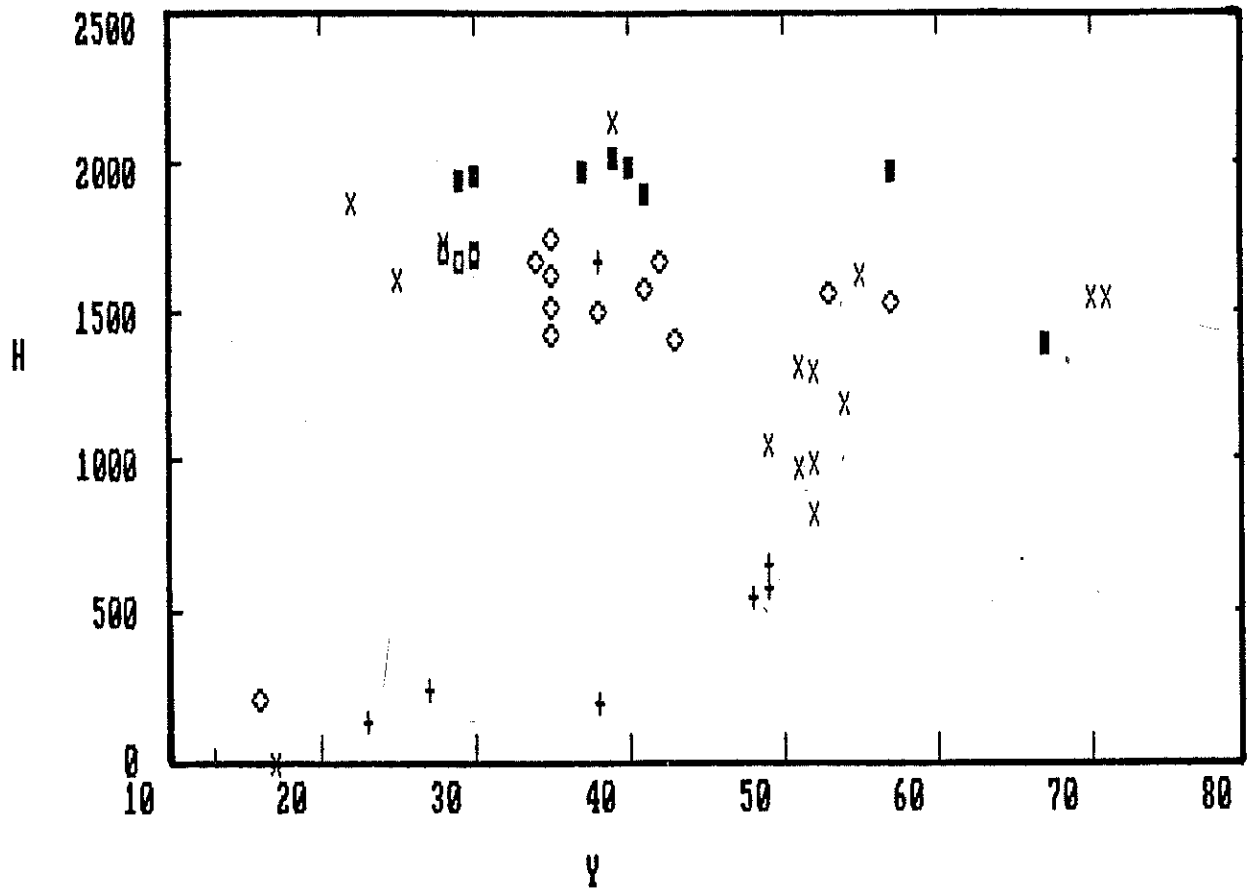
FIGURE 15
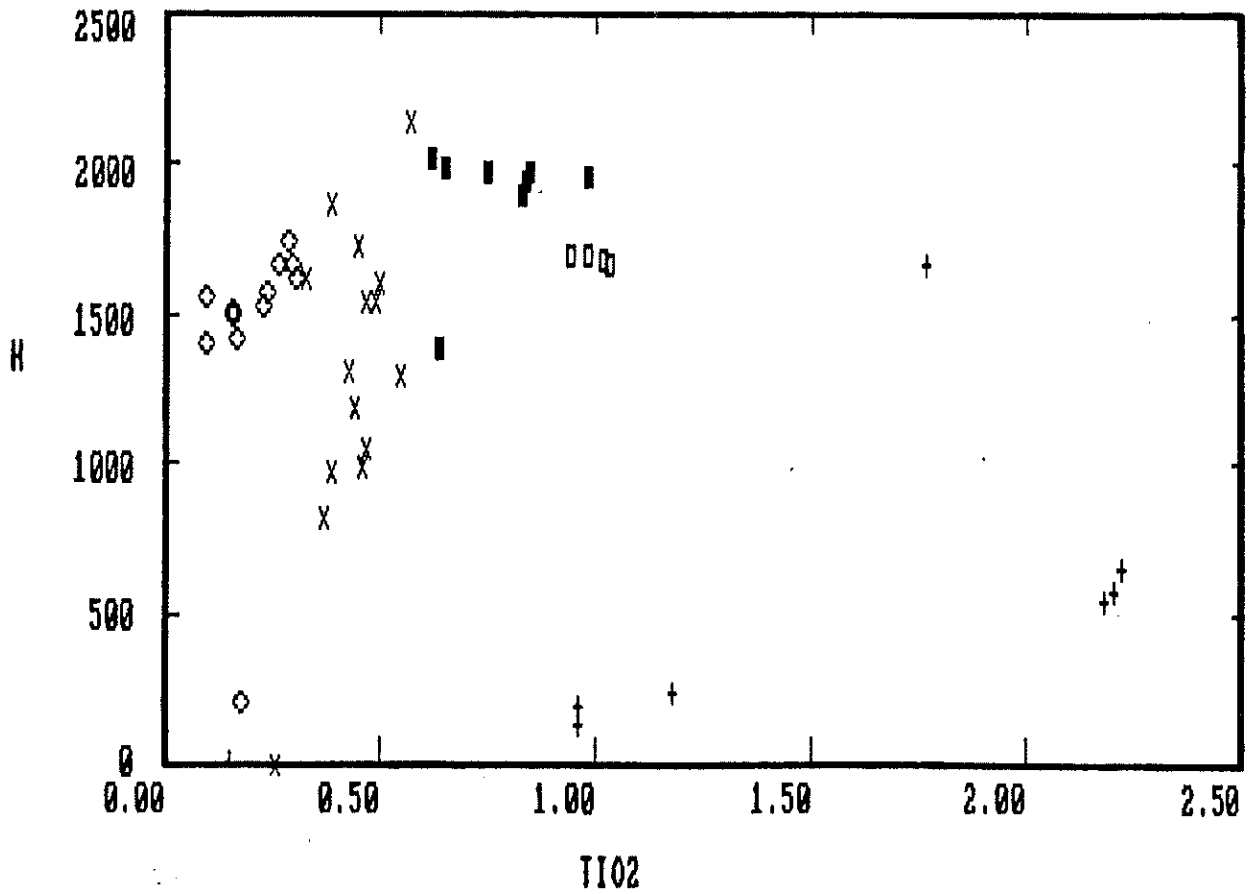
	0%	5%	10%	15%	25%	30%	35%	40%	50%	65%	75%
SiO2	53.11	55.02	55.11	55.21	55.42	55.53	55.65	56.24	57.9	61.76	66.63
TiO2	1.18	1.28	1.35	1.42	1.61	1.72	1.84	1.84	1.78	1.64	1.45
Al2O3	15.63	15.5	15.26	15	14.42	14.14	13.84	13.71	13.53	13.32	13.4
Fe2O3	2	2.16	2.28	2.41	2.71	2.89	3.09	3.04	2.79	2.27	1.65
FeO	7	7.57	7.77	7.97	8.41	8.64	8.89	8.84	8.55	7.88	7.08
FeO*				10.14	10.85	11.24	11.67	11.57	11.06	9.92	8.56
MgO	6.16	6.61	6.34	6.05	5.46	5.13	4.81	4.55	4.02	2.99	2.13
CaO	8.18	8.1	8.06	8.02	7.9	7.78	7.61	7.38	6.69	4.7	1.88
Na2O	2.75	2.82	2.85	2.87	2.9	2.92	2.92	2.95	2.99	2.95	2.61
K2O	0.86	0.93	0.98	1.04	1.17	1.25	1.34	1.45	1.74	2.49	3.47
Temperature		1176.9	1171.5	1165.8	1153.2	1146.5	1139.4	1134.6	1125.3	1107.1	1092.9
Liquid fraction		94.93	89.84	84.95	74.94	69.96	64.97	59.97	49.99	34.97	24.99
Magnetite %								0.37	1.25	2.47	3.25
Ca-poor pyroxene%		0.09	0.09	3.69	7.21	8.73	10.21	11.21	12.92	14.57	15.48
Augite %		0.48	0.48	0.48	0.71	1.07	1.61	2.48	4.67	8.67	12.07
Plagioclase %		4.49	7.63	10.87	17.1	20.21	23.18	25.93	31.13	38.95	44.14
COMPOSITION											
Magnetite MT-USP								48-48	48-47	48-44	48-39
Ca-poor pyroxene En-Fs		85-85	85-84	85-82	85-79	85-77	85-75	85-74	85-81	85-86	85-58
Augite Di-Hd		84-84	84-84	84-84	84-86	84-79	84-77	84-76	84-74	84-70	84-64
Plagioclase An-Ab		71-68	71-67	71-66	71-63	71-69	71-59	71-57	71-53	71-63	71-32

SOLIDUS TEMPERATURE Ca poor pyroxene = 1176.9, Plagioclase = 1188.8, Augite = 1177.9, Magnetite = 1137.2.

TABLE 1   Fractional crystallizing magma modelling (Nathan and Kirk,1978) from an initial basaltic composition (Mg rich basalt, sample 908-118).
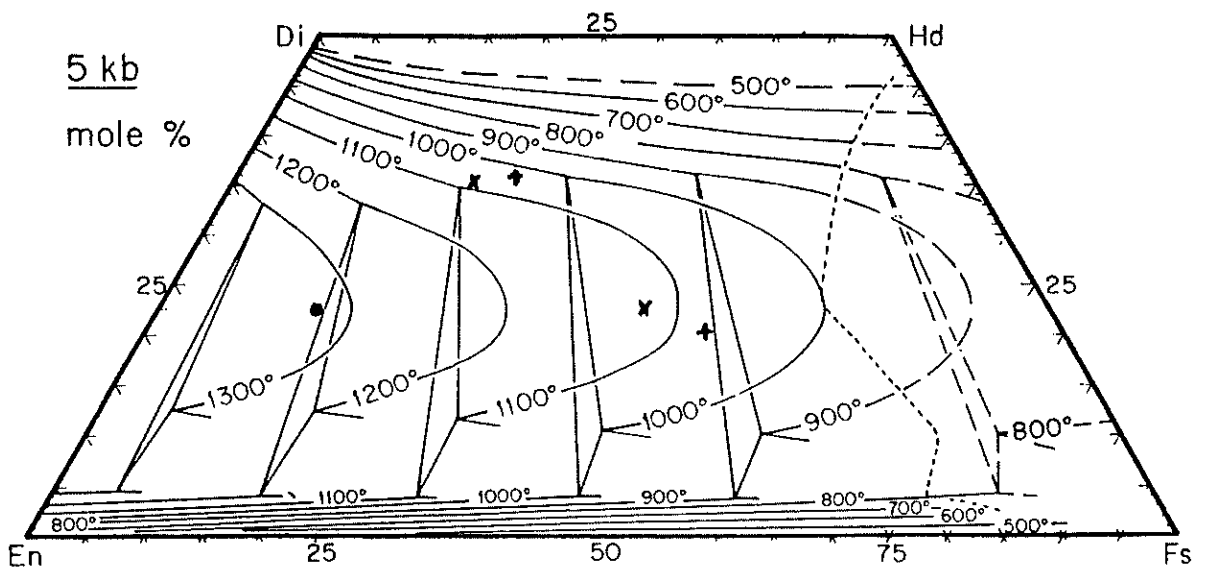
FIGURE 16   Pyroxene thermometry using polythermal

orthopyroxene + augite, orthopyroxene + augite +

pigeonite, and pigeonite + augite relations at 5

Kb (from Lindsley, 1983). Raw data of pyroxene

compositions have been projected as outlined by

Lindsley (1983).

KEY

●   Basalt   (Mg rich; 908-123)

+   Basalt   (Mg poorer; (908-150)

X   Andesite   (908-146)

BASALT 908-111 TO BASALT 908-021

COMPOSITION	SOLUTION	% CUMULATE
908-111	1	
LAB-15	-0.21	53.694
-123-A	-0.182	46.304
908-021	0.608	

R-SQUARED= 6.312

BASALT908-021 TO RHYODACITE 908-111

COMPOSITION	SOLUTION	%CUMULATE
908-021	1	
-150PI	-0.246	36.179
PL-123	-0.349	51.354
-123 M	0.036	-5.287
AP-150	-0.031	4.567
-150 I	-0.09	13.188
908-111	0.32	

R-SQUARED= 4.064

DACITE 908-064 TO RHYODACITE 908-105

COMPOSITION	SOLUTION	%CUMULATE
908-064	1	
AND-150	-0.052	20.677
K-SP-111	-0.113	44.863
-150 AUG	-0.058	23.17
150-ILM	-0.028	11.289
908-105	0.749	

R-SQUARED= 0.399

BASALT908-061-ANDESITE 908-053

COMPOSITION	CUMULATE	% CUMULATE
908-061	1	
123-MAG	-0.065	18.65
PL-123	-0.202	57.55
ILMENITE	-0.024	6.88
-123 MAG	-0.059	16.91
908-053	0.649	

R-SQUARED= 1.484

RHYODACITE 908-111 TO RHYOLITE 908-001

COMPOSITION	SOLUTION	% CUMULATE
908-111	1	
-151	-0.03	8.965
K-SP-1	-0.28	84.941
-150 I	-0.018	5.317
AP-150	-0.003	0.776
908-001	0.67	

R-SQUARED= 1.188

TABLE 2   Least squares mixing calculations of possible fractionation trends for representative samples from Kokatha.

FOR MORE COMPREHENSIVE DATA SEE APPENDIX 5

FIGURE 17   Discrimination diagram of Pearce and Cann, (1973)

using Ti, Zr and Sr. The basalts and andesites

from Kokatha plot in the calk-alkaline field.

(OFB = Ocean Floor Basalt, IAB = Island Arc

Basalt, CAB = Calk-alkaline Basalt).

FIGURE 18   Discrimination diagram of Pearce and Cann, (1973)

using Ti, Y and Zr. The basalts and andesites

plot within the calk-alkaline field.

(OFB = Ocean Floor Basalt, LKT = Low K-Tholeiite,

CAB = Calc-alkalin Basalt, WPB = Within Plate

Basalt).

FIGURE 19   Discrimination diagram of Miyashiro, (1974) using

TiO_2 vs FeO^*/MgO. The basalts plot near the

tholeiite and calc-alkaline boundary. The

andesite plots within the calc-alkaline field.

KEY

+   Basalts

▯   Andesites

FIGURE 17

Ti/100

OFB   IAB

CAB

Zr   Sr/2

FIGURE 18

Ti / 100

OFB = B
LKT = A,B
CAB = B,C
WPB = D

D   A

B

C

Zr   Y * 3

FIGURE 19

4

TiO2

Th

OB

CA

0

0   FeOx / MgO   4
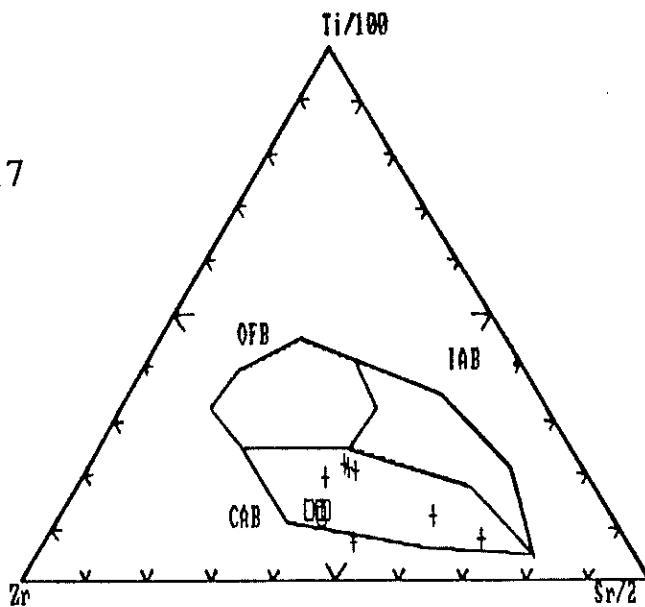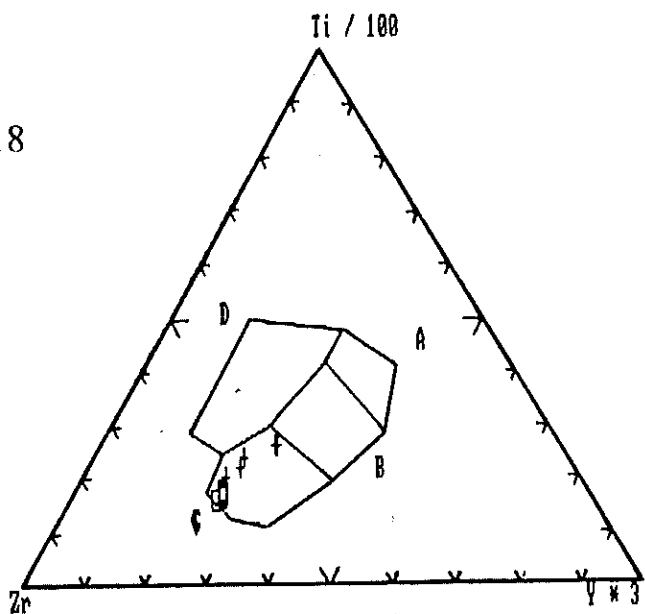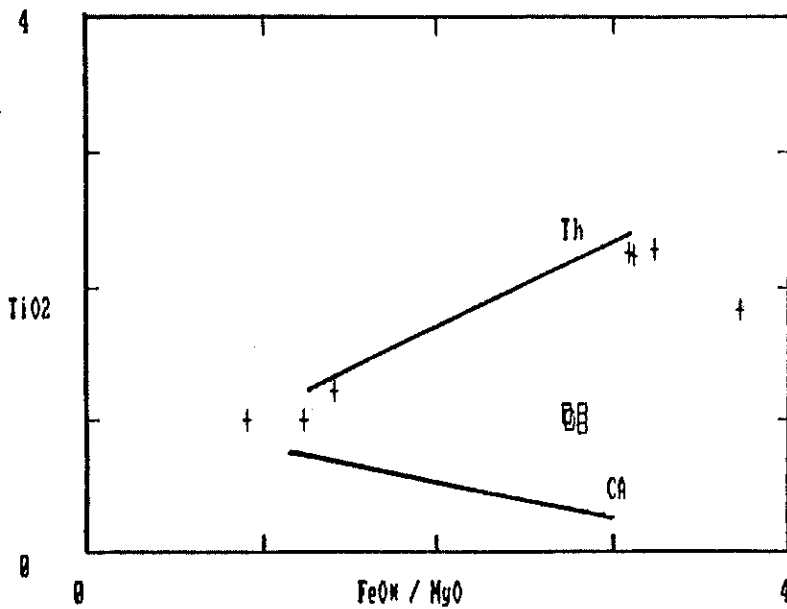
CHAPTER 6 ISOTOPIC DATA

6.1 INTRODUCTION

In the following chapter, strontium and neodymium isotopes are used to determine model and isochron ages of the rocks with implications of possible sources. Detailed information is supplied in appendix 4. Samples have been chosen on their freshness and their rocktype to give the minimum alteration effects and the widest possible range of values. Samples analysed include 908-150 (basalt BW), 908-18 (andesite AE), 908-106 (dacite/rhyodacite D1) and 908-1 (rhyolite ignimbrite RH3). An additional sample K5 (basalt BW) was supplied by Kathy Stewart (PhD Thesis in prep).

6.2 STRONTIUM

Previous Rb-Sr data indicate an age of 1525 ± 14 Ma for rocks in the Kokatha region. There has, however been suggestion that the age of the rocks are somewhat older than this date (Webb et al.,1986). Sr^{87}/Sr^{86} vs Rb^{87}/Sr^{86} for 5 samples over a range of rocktypes has been plotted (fig.20). A Rb-Sr isochron can be drawn giving an age of 1588.4 ± 31.6 Ma with an initial ratio of .70558. This date is somewhat older than previous isochron ages supporting the notion that the lower Gawler Range Volcanics are indeed significantly older.

An interesting point from the Rb-Sr isotopic data is that rocks from both stratigraphic evolutionary cycles lie on a common line to produce an isochron. This suggests melting of the source formed a homogeneous liquid giving any fractionated component the same initial Sr^{87}/Sr^{86} ratio, or if the sources of mafic and felsic magmas were different then isotopic homogenisation took place early in the history of the volcanic pile. The same initial ratio for

rocks from different cycles suggest the source for both fractionating bodies were the same. Evidence for mixed source rocks for felsic and mafic melts does not seem apparent using Rb-Sr systematics.

Figure 21 plots Sr^{87}/Sr^{86} vs time past in billion years. The straight line connecting BABI (Best Achondrite Basaltic Initial) to a present day value of 0.702 (Faure,1986), represents strontium evolution mantle regions depleted in Rb. Hypothetical evolutionary paths of Sr ratios in the undepleted mantle give higher ratios of up to 0.706 at present day time (see Faure, 1986). Sr^{87}/Sr^{86} evolutionary paths have been plotted for samples from Kokatha. The initial ratio of 0.70558 clearly lies above the mantle's evolutionary path (even the hypothetical curves mentioned, not shown here) suggesting these rocks are not purely evolved from a contempory mantle source.

The Glenloth Granite near Lake Harris, is a gneissic body of intermediate to acid composition. It has been dated at 2350 ± 33 Ma with an initial Sr^{87}/Sr^{86} ratio of 0.7028 ± 0.0006 (Webb & Thomson, 1977). A range of analyses from the Glenloth Granite gneisses are shown on figure 21. It can be seen that all the samples have a Sr^{87}/Sr^{86} ratio at time 1588.4 Ma which is greater than the initial ratio of the Kokatha samples. The least Rb-enriched samples only exceed the Kokatha initial ratio by about 0.001.

The initial ratio of the Glenloth Granite Suite represents the isotopic composition of the source of the suite at that time. A melt from this source (ie Glenloth Granite Suite) would be expected to be comparatively enriched in Rb hence evolutionary paths of Sr^{87}/Sr^{86} ratios would have a higher gradient than the source material. Hence the source material for the Glenloth Granite Suite would be isotopically consistent with being a source for the Kokatha

rocks with an initial ratio of .70558 at time 1588.4 Ma.

From figure 21 a possible mixture of partial melts of Glenloth Granite and mantle material could be mooted. The Glenloth Granite (higher Sr^{87}/Sr^{86} than Kokatha rocks) and mantle (lower $Sr^{87}Sr^{86}$ than Kokatha rocks) melts could mix in such a proportion to give rise to an intermediate Sr^{87}/Sr^{86} ratio similar to the initial ratio of the Kokatha samples. However it seems likely that two cycles are present at Kokatha suggesting two generations of magma bodies. Initial ratios of rocks from both cycles are identical. A mixing of Glenloth Granite melts (or any other continental material) with mantle melts to produce two bodies with identical Sr^{87}/Sr^{86} is unlikely. Melts of the same source material, however, could be expected to generate the same initial ratio. This would allow an isochon age to be determined using rocks from different evolutionary cycles.

6.3 NEODYMIUM.

Model ages of approximately 2.37 Ga for the rhyolite and the andesite and an age of 2.27 Ga for the basalt (K5 low Mg) are shown in figure 22 plotted against Nd.

The model ages for neodymium are somewhat older than the age of the extrusion of the volcanics (1.59 Ga). A model age for neodymium of 1.59 Ga would suggest fractionation of partial melts from the asthenosphere (see fig.22). This however is not the case suggesting partial melts from the lower crust are involved.

A mixture of lower crustal melts and basalts from the asthenosphere is consistent with Nd isotopic data. Nd model ages of the lower crust may be greater than 2.37 Ma. A basaltic melt from the asthenosphere (age 1.59 Ga) assimilating with the lower crust could be expected to give model ages younger than the lower

crust but older than melts from the asthenosphere at the time of extrusion.

6.4 DISCUSSION

Strontium isotope data favours a melt of lower crust forming a homogeneous magma with little or no compositional input from asthenospheric derived basalts. Neodymium data however suggests assimilation of lower crustal melts and asthenospheric derived basalts to form a homogeneous magma is likely. The role of basaltic melts from the asthenosphere in providing a likely heat source for voluminous magmatism is not under question.

6.5 MODEL FOR VOLCANISM

Many models for the generation of voluminous volcanism and magmatism have been produced. A possible model for volcanism at Kokatha is presented here, largely based on models by Hildreth (1981), Huppert and Sparkes (1988) and Gans et al. (1989). The model is illustrated in figure 23.

Initially a flux of mantle derived basalt enters the lower crust. The lower crust is close to its solidus allowing small increments of basalt input to produce large volumes of partial melt (Sonders et al., 1987). Early within this stage some melts may reach the surface. Once melting of the lower crust occurs basaltic melts become pooled in the lower crust due to density contrasts. Mixing of the two melts may or may not occur however a homogeneous voluminous magma body is formed.

Diaparism of the homogeneous melt can proceed due to a lower density than surrounding colder rocks allowing the formation of upper crustal magma chambers. Fractional crystallization and mixing of fractionated components produces compositionally layered

magma chambers.

Eruption of the magma results in a basaltic - andesitic - dacitic/rhyodacitic - rhyolitic stratigraphic series of rock units being deposited.
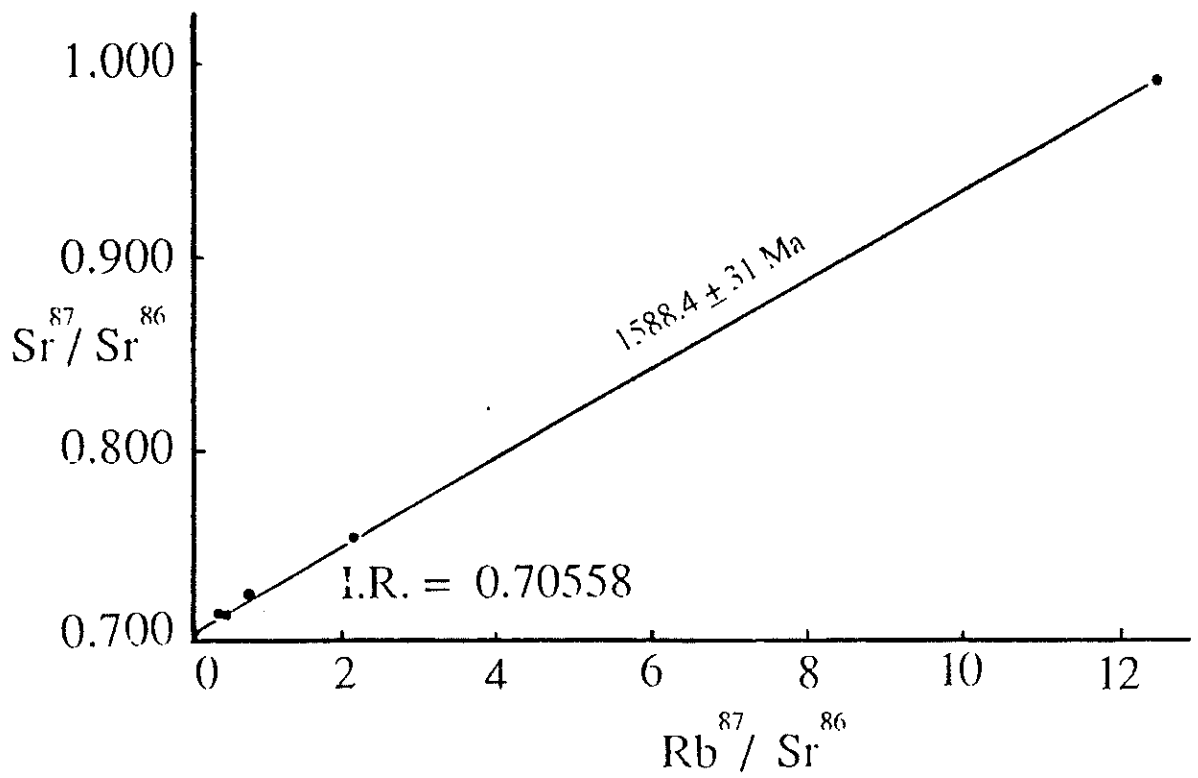
FIGURE 20   Rb-Sr isochron for 5 samples from Kokatha.
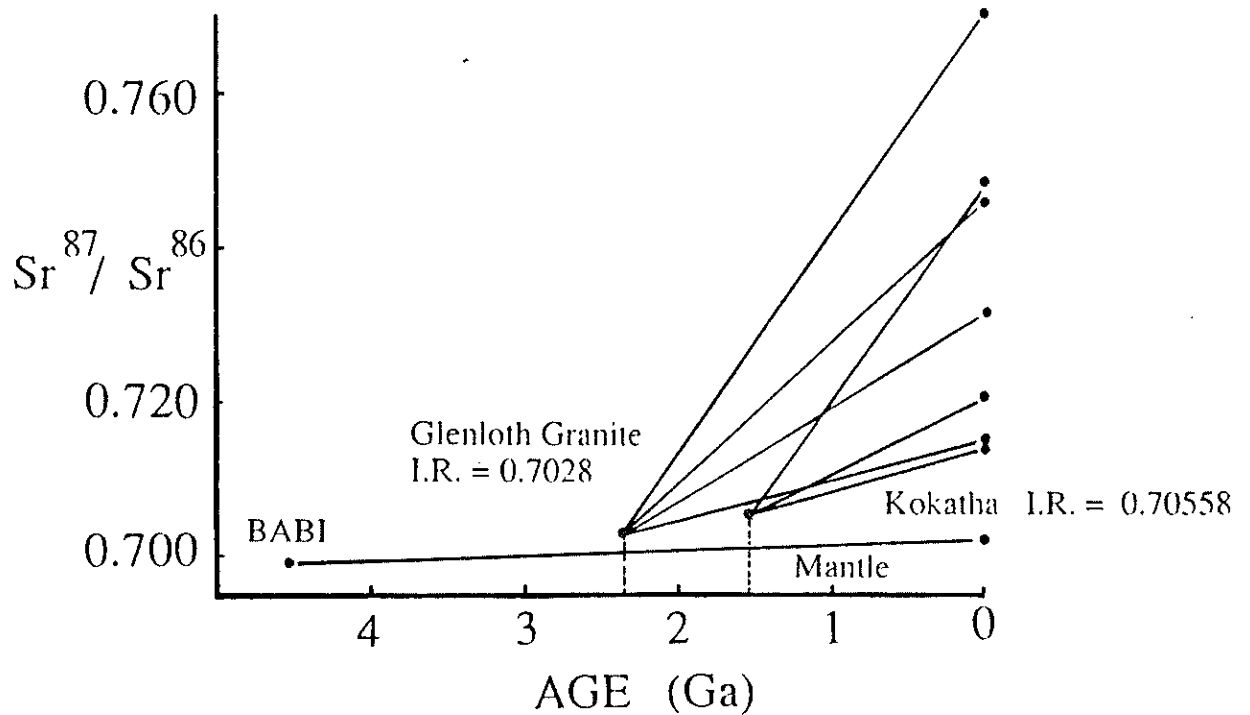
FIGURE 21 Sr^{87}/Sr^{86} vs Age plot for the Glenloth Granite Suite, Kokatha rocks and BABI (Best Achondrite Basaltic Initial).
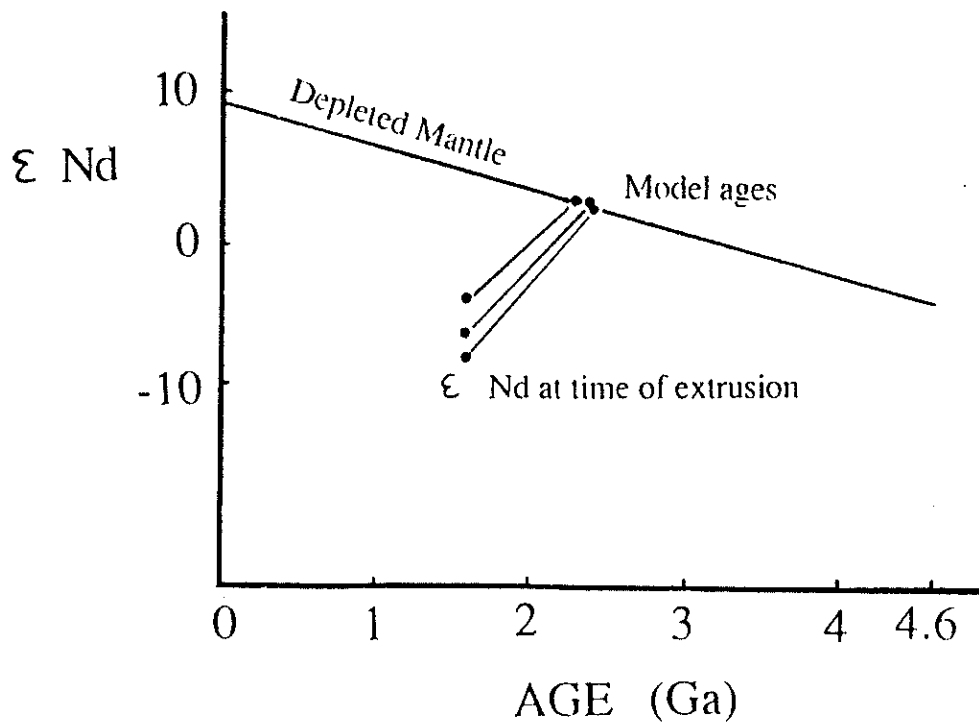
FIGURE 22   Neodymium model ages vs   Nd for rocks from Kokatha.
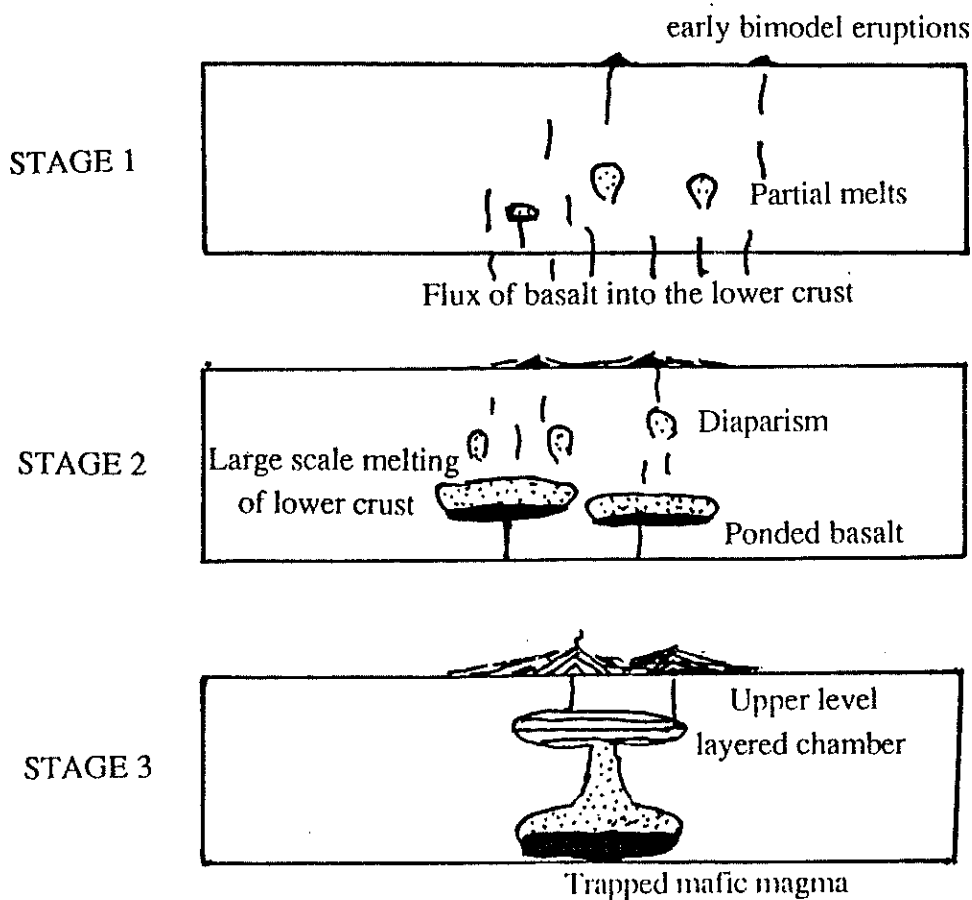
FIGURE 23   Cartoon depicting a possible simplified model for the volcanics seen at Kokatha.

ACKKNOWLEDGEMENTS

REFERENCES

Blissett,A.H.,1975.   Rock units in the Gawler Range Volcanics,

   South Australia: Q. Geol. Notes, Geol. Surv. S. Aust., 55.

   P. 2-14.

Blissett,A.H., and Radke,F., 1979.   The Gawler Range Volcanics -

   a regional review, in, The Gawler Craton, a symposium volume

   compiled by A.J.Parker. P. 45-48.

Branch,C.D., 1978.   Evolution of the Middle Proterozoic

   Chandabooka Caldera, Gawler Range acid volcano-plutonic

   province, South Australia: J. Geol. Soc. Aust., 25. P. 199-

   218.

Cas,R.A.F., and Wright,J.V., 1987.   Volcanic successions : Modern

   and ancient. Allen and Unwin, London. P. 528.

Cooper,J.A, Fanning,C.M., Flook,M.M., and Oliver,R.L., 1976.

   Archean and Proterozoic rocks on southern Eyre Peninsula,

   South Australia: Geol. Soc. Aust., J.23, P.287-292.

Cooper,J.A., Mortimer,G.E., Rosier,C.M., and Uppill,R.K., 1985.

   Gawler Range magmatism - further isotopic age data: Aust. J.

   Earth Sci., 32. P. 115-123.

Cox,K.G., Bell,J.D., and Pankhurst,R.J., 1979. The interpretation

   of igneous rocks.   Allen and Unwin. London. P.450.

Daly,S.J, Webb,A.W., and Whitehead,S.G., 1978.   Archean to early

   Proterozoic banded iron formations in the Tarcoola region,

   South Australia: R. Soc. S. Aust., Trans., 102. P. 141-149.

Ehlers,E., and Blatt,M., 1982.   Petrology Igneous, sedimentary

and metamorphic. Freeman and Co. USA. P.524.

Fanning,C.M., Flint,R.B., Parker,A.J., Ludwig,K.R., and

Blissett,A.H., 1988. Refined Proterozoic evolution of the

Gawler Craton, South Australia, through U-Pb zircon

geochronology: Precambrian Research., 40/41. P. 363-386.

Faure,G., 1986. Principles of isotope geology. 2nd Ed. Wiley,

New york. P.589.

Gans,P.B., Mahood,G.A., and Schermer,E., 1989 (in press).

Synextensional magmatism in the Basin and Range province ; A

case study from the eastern Great Basin. Geol. Soc. of Am.

Special Paper 223, P.(?).

Giles,C.W., 1988. Petrogenisis of the Proterozoic Gawler Range

Volcanics, South Australia. Precambrian Research, 40/41. P.

407-427.

Glen,R.A., Lang,W.P., Parker,A.J., and Rutland,R.W.R., 1977.

Tectonic relationships between the Proterozoic Gawler and Willyama

Orogenic domains, Australia. J. Geol. Soc. Aust.,24. P.125-150.

Hildreth,W., 1979. The Bishop Tuff: Evidence for the origin of

compositional zonation in silicic magma chambers. Geol. Soc. of

Am. Special Paper 180. P.43-75.

Hildreth,W., 1981. Gradients in silicic magma chambers. Implications

for lithospheric magmatism. J. Geophys. Res., 86. P.10153-

10192.

Huppert,H.E., and Sparkes,S.J., 1988. The generation of granitic

magmas by intrusion of basalt into continental crust. Journal of

Petrology, 29. P.599-624.

Lindsley,D.H., 1983. Pyroxene thermometry. Am. Min., 68.
P.477-493

Lipman,P.W., 1975. Evolution of the Platoro Caldera complex and
related volcanic rocks, southeastern San Juan Mountains,
Colorado: Prof. Pap. U.S. Geol. Surv., 852. P.

Lipman,P.W., 1984. The roots of ash flow calderas in western
North America: Windows into the tops of granitic batholiths.
Journal of Geophysical Research, 89. P.8801-8841.

Lowder,G.G., 1972b. Stratigraphy and petrology of the Gawler
Range Volcanics (Project 1/1/144). Progress report No.2.-
Petrology and chemistry of samples from the Kokatha area,
GAIRDNER 1:250000 Sheet. AMDEL report MP 1586/73. S. Aust. Dept.
Mines and Energy open file Env. 2038 (unpublished).

Lowder,G.G., 1973a. Stratigraphy and petrology of the Gawler
Range Volcanics (Project 1/1/144). Progress report No.3.-
Petrology and chemistry of selected samples of the Gawler Range
Volcanics, GAIRDNER 1:250000 Sheet. AMDEL report MP 3072/73.
S. Aust. Dept. Mines and Energy open file Env. 2038 (unpublished).

Mason,B., and Moore,C.B., 1982. Principles of geochemistry 4th
edition. Wiley, New York. P.350.

Mortimer,G.E., Cooper,J.A., and Oliver,R.L., 1986. The
geochronological and geochemical evolution of the Proterozoic
Lincoln Complex, Eyre Peninsula, South Australia: Geol. Soc.
Aust. Abst., 15. P. 140-141.

Myashiro,A., 1974. Volcanic rock series in island arcs and
active continental margins. Am. J. Sci., 274. P.321-355.

Nash,W.P., and Crecraft,H.R, 1985. Partition coefficients for
   trace elements in silicic magmas. Geochimica et Cosmochimica
   Acta, 49. P.2309-2322.

Nathan,H.D., and Kirk,C.K., 1978. A model of magmatic
   crystallization. Journal of Petrology, 19. P.66-94.

Parker,A.J., Fanning,C.M., and Flint,R.B., 1981. Archean to
   Middle Proterozoic geology of the Gawler Craton, South
   Australia. Excursion Guide: S. Aust. Dept. Mines and Energy
   Rep. 81/91 (unpublished).

Parker,A.J., Fanning,C.M., and Flint,R.B., 1985. Geology, in,
   Natural history of Eyre Peninsula, edited by C.R. Twidale,
   M.J. Tyler and M. Davies. R. Soc. S. Aust. Occas., 5. P.21-45.

Parker,A.J., and Lemon,N.M., 1982. Reconstruction of the Early
   Proterozoic stratigraphy of the Gawler Craton, South Australia.
   Geol. Soc. Aust., 29. P. 221-238.

Pearce,J.A., and Cann,J.R., 1973. Tectonic setting of basic
   volcanic rocks determined using trace element analysis. Earth
   and Planet. Sci. Lett., 19. P.290-300.

Sims,P.K., 1979. Precambrian subdivided. Geotimes, 24. P. 15.

Sonders,L.J., England,P.C., Wernicke,B.P., and Christiansen,R.L.,
   1987. A physical model for Cenezoic extension of western North
   America, in, Continental extensional tectonics, edited by
   M.P.Dewey, and J.F.Hancock. Geol. Soc. of London, Publication 28.
   P.187-202.

Webb,A.W., 1980a. A geochronological investigation of the

tectono-magmatic hisory of the Gawler Craton. Geol. Soc. Aust.,
27. P. 187-193.

Webb,A.W., and Thomson,B.P., 1977. Archean basement rocks in the
Gawler Craton, South Australia. Search, 8. P. 34-36.

Webb,A.W., Thomson,B.P., Blissett,A.H., Daly,S.J., Flint,R.B.,
and Parker,A.J., 1986. Geochronology of the Gawler Craton,
South Australia. Aust. J. Earth Sci., 33. P.119-143.

Whitney,J.A., and Stormer,J.R., 1985. Mineralogy, petrology and
magmatic conditions from the Fish Canyon Tuff, central San
Juan volcanic field, Colorado. Journal of Petrology, 26.
P.726-762.

APPENDIX 1

SAMPLE LOCATIONS AND BRIEF THIN SECTION DESCRIPTIONS

LOCATION MAP OF ANALYSED SAMPLES

Polished thin sections

908-17   Accretionary lapilli TU3

908-40   Epiclastic VL2

908-44   Rhyodacite RH1

908-68   Dacite GMD

908-80   Dacite RD1

908-91   Volcaniclastic VL3

908-94   Tuff RH4

908-121 Tuff BW

908-122 Rhyodacite BW

908-123 Basalt BW

908-137 Rhyodacite RD1

908-142 Dacite RD1

908-146 Andesite AE

908-150 Basalt BW

Normal thin sections

908-1   Rhyolite ignimbrite RH3

908-3   Rhyodacite RD1

908-18   Andesite AE

908-20   Rhyodacite RD2

908-39   Epiclastic TU4

908-42   Rhyolite ignimbrite BF

908-43   Ash fall tuff RH2

908-50   Epithermal quartz FRH

908-53   Andesite AE

908-55   Rhyolite RH4

908-58   Dacite D1

908-60   Tuff VL4

908-71   Basalt BW

APPENDIX 2

ELECTRON MICROPROBE ANALYSIS OF MINERAL COMPOSITIONS

Polished thin sections were coated with a thin veneer of carbon. Analysis of grains within the sections were carried out using a KEVEX 7000 serves Energy Dispersive System (EDS) attached to a JEOL 733 Analyser. Analyses conditions used were 15KV accelerating voltape and SuA electrom beam current with data being corrected outline using PIBS style software.

Calibration of the KEVEX EDS system was carried out using pure copper as a primary standard.

Samples analysed are as follows:

908 - 44   Rhyolite RH1

908 - 111   Rhyodacite-B RD1

908 - 122   Rhyodacite BW1

908 - 123   Basalt BW (lower)

908 - 137   Rhyodacite-R RD1

908 - 146   Andesite AE

908 - 150   Basalt BW (higher)

	OR	OR	OR	OR	OR	AB	K-SP	OR	OR	
SiO2	63.96	66.30	68.34	66.14	66.97	67.90	67.15	66.68	65.21	
TiO2	0.28	0.20							0.21	
Al2O3	18.37	18.80	19.27	18.70	18.64	21.24	19.05	18.95	18.62	
Fe2O3										
FeO										
MnO										
MgO						0.12				
CaO						1.72				
Na2O	0.25	0.74	0.26	0.62	0.67	10.55	1.53	0.63	0.25	
K2O	15.79	15.97	16.90	15.93	16.34	0.15	14.88	16.22	15.60	
Total	98.7	102.0	104.8	101.4	102.6	101.7	102.6	102.5	99.9	0.0
Si	2.990	2.996	3.007	3.004	3.010	2.925	3.002	3.000	3.001	
Ti	0.010	0.007	0.000	0.000	0.000	0.000	0.000	0.000	0.007	
Al	1.012	1.001	1.000	1.001	0.988	1.079	1.004	1.005	1.010	
Fe3+	0.000	0.000	0.000	0.000	0.000	0.000	0.000	0.000	0.000	
Fe2+	0.000	0.000	0.000	0.000	0.000	0.000	0.000	0.000	0.000	
Mn	0.000	0.000	0.000	0.000	0.000	0.000	0.000	0.000	0.000	
Mg	0.000	0.000	0.000	0.000	0.000	0.008	0.000	0.000	0.000	
Ca	0.000	0.000	0.000	0.000	0.000	0.079	0.000	0.000	0.000	
Na	0.023	0.065	0.022	0.055	0.058	0.881	0.133	0.055	0.022	
K	0.942	0.921	0.949	0.923	0.937	0.008	0.849	0.931	0.916	
Total	4.976	4.989	4.978	4.984	4.994	4.980	4.987	4.991	4.956	0.000

	ab	k-sp	k-sp	ab	or	k-sp-sc	ab	or	g-mass	
SiO2	62.98	61.98	60.95	60.81	63.51	65.19	66.05	64.69	72.90	
TiO2		0.17	0.10		0.40	0.09			0.30	
Al2O3	21.22	17.68	17.41	19.45	18.40	19.10	21.33	18.50	12.77	
Fe2O3										
FeO						0.76			1.80	
MnO	0.15									
MgO						0.14			0.27	
CaO	1.99			1.80		0.77	1.92		0.55	
Na2O	9.82	3.27	3.83	10.71	0.25	7.10	10.43	0.58	3.98	
K2O	0.70	11.41	9.54	0.80	15.49	5.29	0.07	15.68	5.36	
Total	96.9	94.5	91.8	93.6	98.1	98.4	99.8	99.5	97.9	0.0
Si	2.867	2.988	2.998	2.881	2.984	2.960	2.903	2.997	3.265	
Ti	0.000	0.006	0.004	0.000	0.014	0.003	0.000	0.000	0.010	
Al	1.139	1.005	1.010	1.086	1.019	1.022	1.105	1.011	0.674	
Fe3+	0.000	0.000	0.000	0.000	0.000	0.000	0.000	0.000	0.000	
Fe2+	0.000	0.000	0.000	0.000	0.000	0.029	0.000	0.000	0.067	
Mn	0.006	0.000	0.000	0.000	0.000	0.000	0.000	0.000	0.000	
Mg	0.000	0.000	0.000	0.000	0.000	0.009	0.000	0.000	0.018	
Ca	0.097	0.000	0.000	0.091	0.000	0.037	0.090	0.000	0.026	
Na	0.867	0.306	0.365	0.984	0.023	0.625	0.889	0.052	0.346	
K	0.041	0.702	0.599	0.048	0.928	0.306	0.004	0.927	0.306	
Total	5.017	5.007	4.975	5.092	4.968	4.992	4.991	4.987	4.713	0.000

	PL	K-SP	PL	OR	PL	PL	AB	AB
SiO2	68.38	64.99	58.87	67.56	63.68	66.04	67.20	67.04
TiO2		0.88						
Al2O3	21.94	19.64	26.92	18.93	25.58	21.73	21.29	21.18
Fe2O3								
FeO			0.40		0.34	0.18		
MnO								
MgO	0.11				0.19	0.12	0.13	
CaO	0.80		8.38		0.73	2.40	1.57	1.56
Na2O	10.66	0.16	7.03	0.36	8.05	9.83	10.89	10.56
K2O	0.99	15.77	0.29	16.64	3.46	0.08	0.22	0.13
Total	102.9	101.4	101.9	103.5	102.0	100.4	101.3	100.5

	PL	K-SP	PL	OR	PL	PL	AB	AB
Si	2.917	2.950	2.593	3.010	2.769	2.887	2.912	2.922
Ti	0.000	0.030	0.000	0.000	0.000	0.000	0.000	0.000
Al	1.103	1.051	1.398	0.994	1.311	1.120	1.088	1.088
Fe3+	0.000	0.000	0.000	0.000	0.000	0.000	0.000	0.000
Fe2+	0.000	0.000	0.015	0.000	0.012	0.007	0.000	0.000
Mn	0.000	0.000	0.000	0.000	0.000	0.000	0.000	0.000
Mg	0.007	0.000	0.000	0.000	0.012	0.008	0.008	0.000
Ca	0.037	0.000	0.395	0.000	0.034	0.112	0.073	0.073
Na	0.882	0.014	0.600	0.031	0.679	0.833	0.915	0.893
K	0.054	0.913	0.016	0.946	0.192	0.004	0.012	0.007
Total	4.999	4.958	5.017	4.981	5.010	4.972	5.008	4.983

	feld	lab	lab	and	k-sp	lab	olig	feld	lab	feld
SiO_2	56.34	53.67	54.51	55.21	54.99	53.32	60.21	52.45	53.43	54.94
TiO_2			0.11							
Al_2O_3	27.83	28.31	27.91	26.56	27.49	28.41	23.55	26.63	28.15	28.15
Fe_2O_3										
FeO	0.64	1.21	1.20	1.11	1.32	1.23	0.71	1.91	0.85	1.40
MnO										
MgO	0.44	0.22	0.31	0.20	0.41	0.23	0.49	0.63	0.36	
CaO	5.60	11.18	10.77	9.19	2.29	11.41	4.87	7.97	10.83	3.88
Na_2O	5.51	5.29	5.39	6.15	5.15	5.03	8.37	4.23	5.33	4.83
K_2O	2.71	0.13	0.17	0.14	5.30	0.11	1.44	2.76	0.14	4.50
Total	99.1	100.0	100.4	98.6	97.0	99.7	99.6	96.6	99.1	97.7
Si	2.559	2.440	2.465	2.531	2.571	2.432	2.712	2.484	2.446	2.547
Ti	0.000	0.000	0.004	0.000	0.000	0.000	0.000	0.000	0.000	0.000
Al	1.490	1.518	1.488	1.435	1.515	1.527	1.250	1.487	1.519	1.539
Fe3+	0.000	0.000	0.000	0.000	0.000	0.000	0.000	0.000	0.000	0.000
Fe2+	0.024	0.046	0.045	0.043	0.052	0.047	0.027	0.076	0.033	0.054
Mn	0.000	0.000	0.000	0.000	0.000	0.000	0.000	0.000	0.000	0.000
Mg	0.030	0.015	0.021	0.014	0.029	0.016	0.033	0.044	0.025	0.000
Ca	0.273	0.545	0.522	0.451	0.115	0.558	0.235	0.404	0.531	0.193
Na	0.485	0.466	0.473	0.547	0.467	0.445	0.731	0.388	0.473	0.434
K	0.157	0.008	0.010	0.008	0.316	0.006	0.083	0.167	0.008	0.266
Total	5.017	5.038	5.028	5.029	5.063	5.030	5.070	5.050	5.035	5.034

	and	and	k-sp	and	lab					
SiO_2	54.78	56.45	61.21	56.73	51.56					
TiO_2			0.27							
Al_2O_3	28.06	26.79	20.13	26.89	27.75					
Fe_2O_3										
FeO	1.01	0.53	1.26	0.61	1.04					
MnO										
MgO	0.25	0.49	1.63	0.29	0.16					
CaO	9.98	7.93	1.65	8.65	11.05					
Na_2O	5.54	6.60	2.28	6.25	5.05					
K_2O	0.38	0.46	10.52	0.61	0.09					
Total	100.0	99.3	99.0	100.0	96.7	0.0	0.0	0.0	0.0	0.0

	and	and	k-sp	and	lab					
Si	2.480	2.557	2.837	2.554	2.425					
Ti	0.000	0.000	0.009	0.000	0.000					
Al	1.498	1.430	1.100	1.427	1.539					
Fe^{3+}	0.000	0.000	0.000	0.000	0.000					
Fe^{2+}	0.038	0.020	0.049	0.023	0.041					
Mn	0.000	0.000	0.000	0.000	0.000					
Mg	0.017	0.033	0.113	0.019	0.011					
Ca	0.484	0.385	0.082	0.417	0.557					
Na	0.486	0.580	0.205	0.546	0.461					
K	0.022	0.027	0.622	0.035	0.005					
Total	5.025	5.031	5.017	5.022	5.039	0.000	0.000	0.000	0.000	0.000

	aug	aug	aug	aug	aug					
SiO2	54.18	54.64	54.55	54.46	55.23					
TiO2				0.26	0.20					
Al2O3	2.80	2.64	2.51	2.80	2.28					
Fe2O3										
FeO	8.38	7.17	8.03	7.75	7.49					
MnO	0.13	0.12	0.16	0.17	0.25					
MgO	18.19	18.86	18.49	18.81	18.87					
CaO	12.78	12.37	12.45	12.48	12.41					
Na2O	0.27	0.36	0.46	0.38	0.46					
K2O		0.06								
Total	96.7	96.2	96.6	97.1	97.2	0.0	0.0	0.0	0.0	0.0

	aug	aug	aug	aug	aug					
Si	2.013	2.026	2.024	2.009	2.031					
Ti	0.000	0.000	0.000	0.007	0.006					
Al	0.123	0.115	0.110	0.122	0.099					
Fe3+	0.000	0.000	0.000	0.000	0.000					
Fe2+	0.260	0.222	0.249	0.239	0.230					
Mn	0.004	0.004	0.005	0.005	0.008					
Mg	1.007	1.042	1.022	1.034	1.034					
Ca	0.509	0.492	0.495	0.493	0.489					
Na	0.019	0.026	0.033	0.027	0.033					
K	0.000	0.003	0.000	0.000	0.000					
Total	3.935	3.930	3.938	3.937	3.930	0.000	0.000	0.000	0.000	0.000

	AB	AB	AB	OR	K-SP	AB	OR	AB
SiO2	69.22	69.40	69.42	66.05	73.06	69.67	67.34	67.79
TiO2				0.27	0.14			
Al2O3	20.11	20.36	20.39	18.79	14.29	20.43	18.07	20.87
Fe2O3								
FeO				0.46	1.12		0.41	
MnO								
MgO			0.16		0.15			0.16
CaO	0.45	0.19	0.72		0.19	0.61		0.56
Na2O	10.83	11.05	11.52	0.29	2.14	11.04	0.12	10.05
K2O	0.13	0.10	0.18	16.18	10.03	0.09	16.02	0.61
Total	100.7	101.1	102.4	102.0	101.1	101.8	102.0	100.0

	AB	AB	AB	OR	K-SP	AB	OR	AB
Si	2.992	2.988	2.967	2.990	3.221	2.982	3.038	2.956
Ti	0.000	0.000	0.000	0.009	0.005	0.000	0.000	0.000
Al	1.025	1.034	1.027	1.003	0.743	1.031	0.961	1.073
Fe3+	0.000	0.000	0.000	0.000	0.000	0.000	0.000	0.000
Fe2+	0.000	0.000	0.000	0.017	0.041	0.000	0.015	0.000
Mn	0.000	0.000	0.000	0.000	0.000	0.000	0.000	0.000
Mg	0.000	0.000	0.010	0.000	0.010	0.000	0.000	0.010
Ca	0.021	0.009	0.033	0.000	0.009	0.028	0.000	0.026
Na	0.908	0.923	0.955	0.025	0.183	0.916	0.010	0.850
K	0.007	0.005	0.010	0.934	0.564	0.005	0.922	0.034
Total	4.953	4.959	5.002	4.979	4.776	4.963	4.947	4.949

	ab	ab	or	ab	or	ab	or	ab	ab	or
SiO2	63.55	69.67	66.06	66.25	61.43	68.18	65.73	67.25	68.62	66.76
TiO2	0.15				0.23					
Al2O3	20.06	20.79	18.48	21.33	17.83	21.06	18.34	20.96	21.09	18.60
Fe2O3										
FeO	0.83	0.14	0.16	0.37				0.20	0.34	
MnO										
MgO	0.20	0.12							0.08	
CaO	1.29	0.63		1.97		1.05		1.25	1.00	
Na2O	10.14	11.73	0.46	10.51	0.83	11.41	0.61	11.11	11.23	0.72
K2O	0.67	0.18	15.90	0.49	14.24	0.24	15.74	0.09	0.19	15.76
Total	96.9	103.3	101.1	100.9	94.6	101.9	100.4	100.9	102.6	101.8

	ab	ab	or	ab	or	ab	or	ab	ab	or
Si	2.898	2.956	3.011	2.894	2.985	2.933	3.013	2.925	2.935	3.015
Ti	0.005	0.000	0.000	0.000	0.008	0.000	0.000	0.000	0.000	0.000
Al	1.078	1.040	0.993	1.098	1.021	1.068	0.991	1.075	1.064	0.990
Fe3+	0.000	0.000	0.000	0.000	0.000	0.000	0.000	0.000	0.000	0.000
Fe2+	0.032	0.005	0.006	0.014	0.000	0.000	0.000	0.007	0.012	0.000
Mn	0.000	0.000	0.000	0.000	0.000	0.000	0.000	0.000	0.000	0.000
Mg	0.014	0.008	0.000	0.000	0.000	0.000	0.000	0.000	0.005	0.000
Ca	0.063	0.029	0.000	0.092	0.000	0.048	0.000	0.058	0.046	0.000
Na	0.897	0.965	0.041	0.890	0.078	0.952	0.054	0.937	0.931	0.063
K	0.039	0.010	0.925	0.027	0.883	0.013	0.920	0.005	0.010	0.908
Total	5.025	5.012	4.975	5.016	4.976	5.015	4.979	5.008	5.004	4.976

	f-aug	f-aug	f-aug	aug	aug	aug				
SiO2	50.75	45.15	49.41	51.52	51.40	52.30				
TiO2	0.20	0.25	0.23	0.48		0.29				
Al2O3	3.20	3.76	3.47	1.95	1.47	0.87				
Fe2O3										
FeO	21.35	20.86	23.45	12.85	14.93	16.23				
MnO	0.55	0.48	0.47	0.47	0.54	0.47				
MgO	10.00	7.69	7.83	14.11	9.86	12.83				
CaO	11.58	10.83	11.43	17.82	19.78	16.31				
Na2O	0.95	0.82	0.83	0.66	0.78	0.84				
K2O	0.28	0.49	0.58			0.06				
Total	98.9	90.3	97.7	99.9	98.8	100.2	0.0	0.0	0.0	0.0
Si	1.975	1.944	1.971	1.943	1.990	1.986				
Ti	0.006	0.008	0.007	0.014	0.000	0.008				
Al	0.147	0.191	0.163	0.087	0.067	0.039				
Fe3+	0.000	0.000	0.000	0.000	0.000	0.000				
Fe2+	0.695	0.751	0.782	0.405	0.483	0.515				
Mn	0.018	0.018	0.016	0.015	0.018	0.015				
Mg	0.580	0.493	0.466	0.793	0.569	0.726				
Ca	0.483	0.500	0.489	0.720	0.820	0.664				
Na	0.072	0.068	0.064	0.048	0.059	0.062				
K	0.014	0.027	0.030	0.000	0.000	0.003				
Total	3.989	4.000	3.987	4.024	4.006	4.018	0.000	0.000	0.000	0.000

	and	lab	lab	feld	and	lab	lab	feld
SiO2	60.84	48.23	56.32	63.02	55.74	55.88	56.48	58.37
TiO2	0.17	0.10	0.10	0.28				0.30
Al2O3	25.79	25.92	28.94	23.80	28.28	28.78	28.81	26.55
Fe2O3								
FeO	0.62	0.78	0.83	0.59	0.76	0.96	0.91	1.21
MnO								
MgO	0.21	0.18	0.16	0.13	0.23		0.19	0.37
CaO	7.26	9.91	11.39	4.90	10.51	11.01	10.76	4.40
Na2O	7.56	4.84	5.61	5.65	5.95	5.43	5.50	5.82
K2O	0.23	0.15	0.18	4.03	0.16	0.22	0.14	3.59
Total	102.7	90.1	103.5	102.4	101.6	102.3	102.8	100.6

	and	lab	lab	feld	and	lab	lab	feld
Si	2.651	2.430	2.467	2.762	2.483	2.474	2.484	2.618
Ti	0.006	0.004	0.003	0.009	0.000	0.000	0.000	0.010
Al	1.325	1.540	1.494	1.230	1.485	1.502	1.494	1.404
Fe3+	0.000	0.000	0.000	0.000	0.000	0.000	0.000	0.000
Fe2+	0.023	0.033	0.030	0.022	0.028	0.036	0.033	0.045
Mn	0.000	0.000	0.000	0.000	0.000	0.000	0.000	0.000
Mg	0.014	0.014	0.010	0.008	0.015	0.000	0.012	0.025
Ca	0.339	0.535	0.535	0.230	0.502	0.522	0.507	0.211
Na	0.639	0.473	0.476	0.480	0.514	0.466	0.469	0.506
K	0.013	0.010	0.010	0.225	0.009	0.012	0.008	0.205
Total	5.007	5.037	5.026	4.967	5.036	5.014	5.008	5.026

	lab	and	feld	and						
SiO2	61.30	56.74	53.19	54.85						
TiO2	0.10	0.22	0.16							
Al2O3	24.54	26.15	27.38	27.09						
Fe2O3										
FeO	0.75	0.88	1.93	1.05						
MnO										
MgO	0.10	0.23	0.45	0.20						
CaO	6.16	7.64	4.57	9.66						
Na2O	8.04	6.67	4.63	5.99						
K2O	0.30	0.91	4.21	0.25						
Total	101.3	99.4	96.5	99.1	0.0	0.0	0.0	0.0	0.0	0.0

	lab	and	feld	and						
Si	2.702	2.574	2.512	2.506						
Ti	0.003	0.008	0.006	0.000						
Al	1.275	1.398	1.524	1.459						
Fe3+	0.000	0.000	0.000	0.000						
Fe2+	0.028	0.033	0.076	0.040						
Mn	0.000	0.000	0.000	0.000						
Mg	0.007	0.016	0.032	0.014						
Ca	0.291	0.371	0.231	0.473						
Na	0.687	0.587	0.424	0.531						
K	0.017	0.053	0.254	0.015						
Total	5.009	5.039	5.059	5.037	0.000	0.000	0.000	0.000	0.000	0.000

	aug	pig	pig	aug	aug	f-aug		
SiO2	53.30	53.55	52.63	53.00	51.74	45.29		
TiO2	0.49			0.14	0.29	0.87		
Al2O3	0.97	1.46	1.94	0.77	1.80	4.47		
Fe2O3								
FeO	14.47	27.07	23.61	14.19	15.79	20.14		
MnO	0.57	1.13	0.89	0.54	0.49	0.25		
MgO	12.09	12.40	12.42	13.36	12.24	8.44		
CaO	20.74	3.57	5.96	18.05	18.38	10.75		
Na2O	0.37	0.55	0.33	0.29	0.40	0.72		
K2O		0.16	0.50		0.12	0.21		
Total	103.0	99.9	98.4	100.5	101.8	90.3	0.0	0.0

	aug	pig	pig	aug	aug	f-aug		
Si	1.971	2.057	2.038	1.992	1.940	1.935		
Ti	0.014	0.000	0.004	0.008	0.025	0.000		
Al	0.042	0.066	0.089	0.034	0.080	0.225		
Fe3+	0.000	0.000	0.000	0.000	0.000	0.000		
Fe2+	0.448	0.870	0.765	0.446	0.495	0.719		
Mn	0.018	0.037	0.029	0.017	0.016	0.009		
Mg	0.666	0.710	0.717	0.748	0.684	0.537		
Ca	0.822	0.147	0.247	0.727	0.739	0.492		
Na	0.027	0.041	0.025	0.021	0.029	0.060		
K	0.000	0.008	0.025	0.000	0.006	0.011		
Total	4.007	3.935	3.938	3.994	4.013	3.988	0.000	0.000

	-122	-122	-122	-122	-122					
SiO2	35.21	33.85	33.12	36.84	34.89					
TiO2	3.39	1.81	0.68	3.46	1.05					
Al2O3	13.69	15.64	16.32	14.58	16.76					
Fe2O3										
FeO	22.33	25.83	25.07	16.52	21.13					
MnO	0.40	0.23	0.29	0.28	0.33					
MgO	8.39	7.05	10.47	12.30	10.46					
CaO										
Na2O	0.34	0.23	0.18	0.21	0.45					
K2O	9.15	8.41	5.58	9.90	8.19					
Total	92.9	93.1	91.7	94.1	93.3	0.0	0.0	0.0	0.0	0.0

Si	5.125	4.979	4.847	5.132	4.977					
Ti	0.371	0.200	0.075	0.362	0.113					
Al	2.349	2.712	2.815	2.394	2.819					
Fe3+	0.000	0.000	0.000	0.000	0.000					
Fe2+	2.718	3.177	3.068	1.925	2.521					
Mn	0.049	0.029	0.036	0.033	0.040					
Mg	1.820	1.545	2.283	2.554	2.224					
Ca	0.000	0.000	0.000	0.000	0.000					
Na	0.096	0.066	0.051	0.057	0.124					
K	1.699	1.578	1.042	1.759	1.491					
Total	14.227	14.287	14.217	14.216	14.308	0.000	0.000	0.000	0.000	0.000

epidote

	-44	-122	-123	-146						
SiO2	37.64	27.26	34.26	36.68						
TiO2		7.93	0.65							
Al2O3	22.29	15.26	20.36	25.20						
FE2O3										
FeO	15.46	22.95	11.75	4.72						
MnO	0.30	0.82	0.29							
MgO	0.53	9.27	0.53	2.20						
CaO	21.10	7.15	19.30	22.90						
Na2O	0.72	0.50	0.50	0.36						
K2O	0.12	0.39	0.08	0.08						
Total	98.2	91.5	87.7	92.1	0.0	0.0	0.0	0.0	0.0	0.0

Si										
Ti										
Al										
Fe3+										
Fe2+										
Mn										
Mg										
Ca										
Na										
K										
Total	0.000	0.000	0.000	0.000	0.000	0.000	0.000	0.000	0.000	0.000

APPENDIX 3

METHOD OF WHOLE ROCK ANALYSIS AND MAJOR ELEMENT AND TRACE ELEMENT

CONCENTRATIONS

Sample prepartion for whole rock analysis:
----

1.   A core of fresh unweathered sample was obtained by trimming
weathered edges off the rock.

2.   Samples were crushed in a jaw crusher.

3.   Crushed samples were ground to a fine powder using a
Siebtechnic tungsten carbide mill.

4.   An accurate amount of sample was placed in a crucible, and
ignited overnight at 960o to drive off volatiles.   The loss on
ignition (LOI) was calculated.

5.   For each sample 280 mg of ignited sample, 20 mg of sodium
nitrate and 1.5 g of flux were weighed out, mixed and used to
produce a fused disc.

6.   Using a pressing vessel and hydraulic press, pressed pellets
of approximately 5g of unignited sample poweder were made.

Major element analysis

Major elements were determined using the Siemens SRS, XRF.
Sodium concentration were determined for each sample by digesting
anaccurate amount of sample (50 - 60 g) in a teflon beaker
containing hydroflouric acid (10 ml).   50% sulphuric acid (2 ml)
and water (10 - 20 ml).   The mixture was heated for 16 hours at
approximately $125^{o}C$ and the resultant solution diluted to 100 ml
withdistilled water and stored in a plastic bottle to prevent
leaching from glass.   The sodium concentration of the solution was
determined using the Varian Techtron Atomic Absorption
Spectrophotometer.

Trace element analysis

Trace element abundances were determined using the Siemens XRF.

Results

Results are tabulated as the following data. Major elements are expressed as weight %. Total iron is given aS Fe_2O_3. Trace elments are expressed in ppm.

	-018	-020	-021	-047	-051	-052	-053	-058	-061	-064
SIO2	60.33	69.71	53.32	67.76	59.68	61.39	60.88	69.52	52.91	64.09
TIO2	1.03	0.43	2.22	0.64	1.02	0.98	0.94	0.57	1.77	0.98
AL2O3	14.10	14.09	14.36	15.10	13.89	14.05	13.81	13.61	14.79	13.90
FE2O3	9.06	3.38	12.06	3.23	8.91	8.31	8.12	4.07	13.60	6.93
FEO	nd	nd	nd	nd	nd	nd	nd	nd	nd	nd
MNO	0.16	0.12	0.23	0.06	0.18	0.15	0.16	0.11	0.24	0.16
MGO	2.98	0.75	3.36	0.26	2.84	2.72	2.59	0.90	3.30	1.59
CAO	4.59	0.74	6.48	1.01	4.34	4.45	4.04	1.71	5.18	2.98
NA2O	3.64	4.21	2.77	4.83	4.41	4.31	4.53	3.64	3.65	4.05
K2O	2.82	5.33	2.74	5.31	2.88	1.86	3.37	4.61	2.51	3.62
H2O+	1.17	0.61	0.64	0.37	0.80	1.22	0.70	0.87	1.36	0.85
H2O-	nd	nd	nd	nd	nd	nd	nd	nd	nd	nd
P2O5	0.22	0.08	1.36	0.11	0.22	0.21	0.21	0.15	0.43	0.27
TOTAL	100.10	99.45	99.54	98.68	99.17	99.65	99.35	99.76	99.74	99.42
SR	389	152	547	222	381	352	382	206	432	359
RB	103.00	174	121	183	111	67.00	121	162	98.00	141
Y	29.00	51.00	49.00	67.00	30.00	30.00	28.00	39.00	38.00	30.00
ZR	207	370	231	367	212	212	211	340	233	239
NB	8.90	17.50	9.20	19.40	8.00	8.20	8.20	13.80	8.80	9.80
BA	1046	2188	1382	1946	975	635	1046	1306	1096	1145
SC	22.00	10.70	30.00	10.70	24.00	20.00	20.00	9.90	27.00	17.00
NI	14.00	2.00	3.00	2.00	15.00	11.00	13.00	4.00	5.00	4.00
V	193	3.00	155	10.00	188	176	172	31.00	282	105.00
CR	1.00	1.00	1.00	1.00	8.00	5.00	12.00	1.00	1.00	1.00
GA	19.00	19.00	23.00	nd	21.00	20.00	21.00	19.00	23.00	20.00
CE	83.00	34.00	107.00	162	81.00	75.00	87.00	117	85.00	93.00
ND	34.00	47.00	66.00	71.00	35.00	33.00	39.00	48.00	45.00	43.00
LA	47.00	76.00	56.00	82.00	42.00	41.00	46.00	62.00	43.00	54.00
TH	8.90	25.00	13.00	27.00	9.70	12.00	11.00	23.00	7.60	13.00
PB	44.00	31.00	14.00	25.00	40.00	34.00	38.00	28.00	19.00	26.00
U	4.10	6.60	5.40	6.20	3.40	4.20	3.30	4.80	2.50	4.60
CU	13.00	1.00	5.00	1.00	13.00	9.00	13.00	1.00	11.00	5.00
ZN	96.00	127	137	41.00	97.00	87.00	88.00	74.00	146	92.00
MG#	47.62	38.02	43.50	18.20	46.84	47.50	46.85	37.93	40.14	38.81
ZR/Y	7.14	7.25	4.71	5.48	7.07	7.07	7.54	8.72	6.13	7.97
K2+NA	6.46	9.54	5.51	10.14	7.29	6.17	7.90	8.25	6.16	7.67
H	1669	1314	662	1382	1679	1687	1697	2139	1655	1951
CE/Y	2.86	.66667	2.18	2.42	2.70	2.50	3.11	3.00	2.24	3.10

```
-018 -      ANDESITE AE
-020 -      RHYODACITE RD2
-021 -      BASALT BN
-047 -      DACITE RD2
-051 -      ANDESITE AE
-052 -      ANDESITE AE
-053 -      ANDESITE AE
-058 -      RHYODACITE D1
-061 -      BASALT BE
-064 -      DACITE GMD
```

	-072	-079	-080	-001	-012	-019	-029	-031	-035	-039
SIO2	53.02	69.46	69.33	76.00	72.08	65.32	71.77	75.59	75.65	68.92
TIO2	2.18	0.46	0.47	0.16	0.47	0.74	0.49	0.10	0.24	0.33
AL2O3	14.14	14.38	14.43	12.11	12.58	14.41	12.74	13.60	12.25	15.85
FE2O3	12.20	3.31	3.16	2.05	3.38	5.68	3.70	1.50	2.14	3.38
FEO	nd	nd	nd	nd	nd	nd	nd	nd	nd	nd
MNO	0.22	0.14	0.09	0.06	0.10	0.15	0.09	0.04	0.06	0.03
MGO	3.53	0.45	0.49	0.21	0.45	1.11	0.29	0.49	0.37	0.60
CAO	6.45	1.20	1.15	0.52	0.70	2.34	1.16	0.09	0.40	0.55
NA2O	3.27	4.26	4.58	2.41	3.66	4.22	3.08	1.05	3.23	1.03
K2O	2.73	5.14	4.79	5.21	5.31	4.30	5.52	5.86	4.11	7.05
H2O+	0.49	0.45	0.45	0.64	0.46	0.88	0.31	1.30	0.81	1.44
H2O-	nd	nd	nd	nd	nd	nd	nd	nd	nd	nd
P2O5	1.33	0.07	0.08	0.03	0.10	0.19	0.10	0.01	0.05	0.08
TOTAL	99.56	99.32	99.02	99.40	99.29	99.34	99.25	99.63	99.31	99.26
SR	506	210	211	41.00	70.00	265	73.00	32.00	84.00	81.00
RB	87.00	171	147	185	214	147	246	327	164	271
Y	48.00	52.00	49.00	35.00	71.00	38.00	70.00	53.00	41.00	55.00
ZR	224	360	365	266	464	293	471	150	228	236
NB	9.80	17.30	18.20	14.10	25.00	12.40	24.00	18.00	14.70	21.00
BA	1585	2338	2412	919	675	1245	739	302	565	796
SC	26.00	12.00	12.60	5.30	8.50	13.50	9.30	3.00	4.40	6.90
NI	3.00	3.00	2.00	2.00	3.00	6.00	4.00	2.00	4.00	5.00
V	143	3.00	4.00	3.00	13.00	49.00	15.00	4.00	9.00	16.00
CR	1.00	1.00	1.00	1.00	1.00	6.00	1.00	6.00	5.00	1.00
GA	21.00	20.00	18.00	nd	nd	nd	nd	nd	nd	nd
CE	114	153	147	133	189	110.00	189	106.00	120	97.00
ND	64.00	66.00	60.00	5.00	81.00	51.00	81.00	69.00	51.00	48.00
LA	59.00	75.00	69.00	67.00	94.00	60.00	94.00	74.00	59.00	51.00
TH	9.90	26.00	25.00	23.00	34.00	17.00	35.00	39.00	27.00	30.00
PB	12.00	38.00	30.00	44.00	42.00	63.00	34.00	24.00	22.00	37.00
U	4.00	4.50	6.20	10.00	11.00	8.00	8.00	5.00	6.00	4.00
CU	3.00	5.00	2.00	5.00	5.00	5.00	6.00	5.00	4.00	9.00
ZN	140	87.00	87.00	52.00	76.00	96.00	86.00	55.00	62.00	67.00
MG#	44.44	27.31	30.00	22.07	26.90	35.07	17.81	47.45	32.34	32.91
ZR/Y	4.67	6.92	7.45	7.60	6.54	7.71	6.73	2.83	5.56	4.29
K2+NA	6.00	9.40	9.37	7.62	8.97	8.52	8.60	6.91	7.34	8.08
H	546	988	1056	1512	1544	nd	1534	1560	1566	1618
CE/Y	2.38	2.94	3.00	3.80	2.66	2.89	2.70	2.00	2.93	1.76

-072 - BASALT BK
-079 - RHYODACITE-R RD1
-080 - RHYODACITE-B RD1
-001 - RHYOLITE IGNIMBRITE RH3
-012 - FLOWBANDED RHYODACITE FR1
-019 - VOLCANICLASTIC VL5
-029 - RHYODACITE BGD
-031 - ~~AIR FALL TUFF~~ TU3 *Epithermal qtz breccia*
-035 - VOLCANICLASTIC VL1
-039 - EPICLASTIC TU4

	-040	-042	-044	-045	-049	-055	-059	-067	-074A	-078
SIO2	73.27	73.27	74.18	77.85	72.32	73.60	65.80	65.71	75.46	75.58
TIO2	0.31	0.23	0.17	0.10	0.50	0.29	0.83	0.85	0.16	0.14
AL2O3	12.63	14.28	12.49	12.27	12.79	12.43	14.42	13.80	12.53	11.77
FE2O3	2.66	2.45	2.36	1.24	3.06	2.61	6.24	6.01	2.08	1.59
FEO	nd	nd	nd	nd	nd	nd	nd	nd	nd	nd
MNO	0.05	0.08	0.11	0.03	0.09	0.08	0.12	0.17	0.07	0.03
MGO	0.80	0.61	0.38	0.35	0.62	0.42	1.46	1.27	0.23	0.16
CAO	0.43	0.63	0.66	0.30	0.99	0.52	1.37	2.67	0.51	0.50
NA2O	3.46	3.06	3.72	2.33	3.84	3.45	3.51	3.55	2.43	3.05
K2O	5.32	4.19	4.78	4.11	4.71	5.27	3.72	4.61	5.38	5.44
H2O+	0.58	1.01	0.31	0.92	0.46	0.58	1.57	0.69	0.59	0.65
H2O-	nd	nd	nd	nd	nd	nd	nd	nd	nd	nd
P2O5	0.06	0.03	0.02	nd	0.09	0.05	0.22	0.26	0.01	0.02
TOTAL	99.57	99.84	99.18	99.50	99.47	99.30	99.26	99.59	99.45	98.93
SR	99.00	55.00	44.00	33.00	191	82.00	291	208	40.00	25.00
RB	168	231	168	231	143	180	138	181	203	345
Y	35.00	57.00	35.00	43.00	25.00	35.00	41.00	57.00	38.00	67.00
ZR	205	307	303	145	231	327	183	399	263	187
NB	14.40	22.00	15.50	21.00	10.90	14.40	14.30	18.60	14.70	20.00
BA	813	477	901	237	1679	1357	1424	1194	895	151
SC	5.40	5.90	6.30	2.40	8.00	8.40	14.70	15.00	5.50	3.10
NI	3.00	6.00	3.00	2.00	5.00	1.00	4.00	7.00	4.00	4.00
V	17.00	9.00	3.00	2.00	20.00	7.00	60.00	46.00	3.00	3.00
CR	1.00	5.00	1.00	1.00	1.00	5.00	9.00	7.00	1.00	1.00
GA	nd	nd	nd	nd	nd	nd	nd	nd	nd	nd
CE	85.00	128	149	144	79.00	110.00	120	151	129	183
ND	38.00	64.00	64.00	72.00	31.00	55.00	52.00	66.00	53.00	87.00
LA	44.00	65.00	75.00	77.00	43.00	56.00	59.00	76.00	67.00	102.00
TH	15.00	29.00	25.00	43.00	10.00	19.00	15.00	25.00	24.00	51.00
PB	34.00	38.00	69.00	28.00	28.00	19.00	9.00	35.00	50.00	33.00
U	5.00	8.00	9.00	10.00	2.00	3.00	4.00	5.00	7.00	8.00
CU	5.00	7.00	13.00	5.00	5.00	5.00	4.00	21.00	6.00	14.00
ZN	86.00	67.00	61.00	39.00	65.00	57.00	113	85.00	56.00	70.00
MG#	45.39	40.76	30.80	43.82	35.90	30.78	39.27	36.87	23.41	21.76
ZR/Y	5.86	5.39	8.66	3.37	9.24	9.34	4.46	7.00	6.92	2.79
K2+NA	8.78	7.25	8.50	6.44	8.55	8.72	7.23	8.16	7.81	8.49
H	1619	1518	1424	1396	1608	1743	1883	1967	1492	nd
CE/Y	2.43	2.25	4.26	3.35	3.16	3.14	2.93	2.65	3.39	2.73

-040 -		EPICLASTIC VL2
-042 -		RHYOLITE BRECCIA FLOW BF
-044 -		RHYOLITE IGNIMBRITE RH1
-045 -		AIR FALL TUFF TU2
-049 -		RHYODACITE RU1
-055 -		RHYOLITE RH4
-059 -		VOLCANICLASTIC VL4
-067 -		DACITE TBD
-074A -		RHYOLITE IGNIMBRITE RH2
-078 -		HILTABA GRANITE

	-083	-090	-091	-093	-094	-104	-105	-106	-107	-111
SIO2	69.78	73.57	75.21	71.25	71.19	65.65	68.00	68.38	65.80	70.74
TIO2	0.55	0.30	0.27	0.45	0.39	0.84	0.62	0.65	0.75	0.37
AL2O3	14.11	12.44	12.31	13.05	12.41	13.95	13.76	13.95	14.23	13.84
FE2O3	3.69	2.73	3.33	3.30	3.48	5.86	4.75	4.80	5.81	3.07
FEO	nd	nd	nd	nd	nd	nd	nd	nd	nd	nd
MNO	0.13	0.05	0.08	0.08	0.09	0.14	0.14	0.10	0.15	0.11
MGO	0.69	0.64	1.10	0.63	0.72	1.45	1.00	0.79	1.23	0.43
CAO	1.42	0.42	1.15	1.02	5.89	2.24	1.93	2.18	2.17	0.81
NA2O	4.17	3.39	2.56	4.80	2.81	4.12	3.63	3.30	3.99	4.26
K2O	4.14	5.46	3.60	3.64	1.54	3.97	4.43	5.15	3.92	5.24
H2O+	0.46	0.33	0.39	1.14	1.09	1.09	0.81	0.30	1.14	0.34
H2O-	nd	nd	nd	nd	nd	nd	nd	nd	nd	nd
P2O5	0.15	0.04	0.05	0.10	0.16	0.26	0.16	0.17	0.18	0.05
TOTAL	99.29	99.37	100.05	99.46	99.77	99.57	99.23	99.77	99.37	99.26
SR	200	82.00	96.00	190	341	322	209	225	237	121
RB	153	173	115	120	60.00	136	157	166	141	172
Y	52.00	34.00	42.00	28.00	22.00	29.00	39.00	40.00	37.00	52.00
ZR	365	325	293	243	214	238	350	345	293	372
NB	17.00	14.80	15.10	12.30	9.60	10.60	14.00	14.30	12.80	17.40
BA	1793	1346	621	1109	586	1213	1203	1332	1149	1982
SC	12.00	6.50	6.60	8.00	9.30	13.60	12.40	11.60	13.60	10.00
NI	1.00	2.00	5.00	4.00	5.00	4.00	8.00	4.00	7.00	3.00
V	15.00	8.00	20.00	28.00	74.00	81.00	38.00	40.00	54.00	5.00
CR	1.00	1.00	6.00	1.00	6.00	6.00	8.00	8.00	12.00	1.00
GA	nd	nd	nd	nd	nd	nd	nd	nd	nd	nd
CE	153	112	186	91.00	78.00	95.00	125	122	107.00	152
ND	73.00	45.00	74.00	36.00	38.00	43.00	54.00	52.00	44.00	62.00
LA	76.00	57.00	93.00	47.00	45.00	52.00	63.00	67.00	49.00	74.00
TH	25.00	17.00	21.00	11.00	12.00	16.00	19.00	19.00	19.00	24.00
PB	29.00	10.00	25.00	20.00	15.00	33.00	22.00	27.00	35.00	29.00
U	7.00	6.00	5.00	4.00	4.00	4.00	5.00	8.00	8.00	9.00
CU	4.00	5.00	5.00	6.00	6.00	7.00	9.00	10.00	13.00	7.00
ZN	92.00	45.00	51.00	51.00	24.00	82.00	89.00	80.00	108.00	80.00
MG#	34.07	39.32	47.73	34.54	36.38	40.61	36.78	31.27	36.91	27.91
ZR/Y	7.02	9.56	6.98	8.68	9.73	8.21	8.97	8.63	7.92	7.15
K2+NA	8.31	8.85	6.16	8.44	4.35	8.09	8.06	8.45	7.91	9.50
R	1294	1661	1659	1717	1867	1935	2009	1983	1973	818
CE/Y	2.94	3.29	4.43	3.25	3.55	3.28	3.21	3.05	2.89	2.92

```
-083 -     AIR FALL TUFF TU1
-090 -     FLOWBANDED RHYOLITE FRH
-091 -     PYROCLASTIC VL3
-093 -     RHYODACITE RH4
-094 -     RHYODACITE RH4
-104 -     DACITE GMD
-105 -     DACITE D1
-106 -     DACITE D1
-107 -     VOLCANICLASTIC VL5
-111 -     RHYODACITE-R RD1
```

	-118	-119	-120	-122	-123	-132	-137	-150	-151	-152
SIO2	53.11	74.07	56.90	71.91	54.50	70.13	69.67	52.99	78.53	71.19
TIO2	1.18	0.18	0.96	0.26	0.96	0.39	0.44	2.20	0.14	0.37
AL2O3	15.63	14.47	12.95	13.84	14.93	14.04	14.09	14.23	10.61	13.84
FE2O3	9.61	1.04	7.96	2.07	8.92	3.16	3.22	12.22	1.31	2.97
FEO	nd	nd	nd	nd	nd	nd	nd	nd	nd	nd
MNO	0.15	0.05	0.14	0.07	0.15	0.10	0.12	0.20	0.02	0.08
MGO	6.16	3.05	7.92	0.74	6.54	1.45	0.41	3.57	0.36	0.41
CAO	8.18	0.36	4.38	1.70	7.09	0.67	0.99	6.56	0.08	0.64
NA2O	2.75	2.19	2.10	3.61	3.32	4.25	4.02	3.27	2.48	4.17
K2O	0.86	3.04	3.07	4.34	1.23	4.99	5.79	2.63	5.29	5.16
H2O+	1.32	2.13	1.40	0.67	1.29	0.65	0.47	0.28	0.46	0.55
H2O-	nd	nd	nd	nd	nd	nd	nd	nd	nd	nd
P2O5	0.44	0.03	0.94	0.09	0.31	0.07	0.07	1.34	0.02	0.05
TOTAL	99.39	100.61	98.72	99.30	99.24	99.90	99.29	99.49	99.30	99.43
SR	714	650	749	296	995	130	186	491	33.00	116
RB	25.00	154	130	133	34.00	160	191	74.00	321	214
Y	27.00	16.00	38.00	17.00	23.00	51.00	54.00	49.00	61.00	50.00
ZR	170	104.00	328	156	164	377	367	226	188	372
NB	8.00	10.00	13.50	11.90	8.10	17.90	18.70	9.90	20.00	17.00
BA	651	1531	1578	933	830	2035	2251	1462	320	1905
SC	26.00	2.80	24.00	5.20	25.00	10.50	11.10	26.00	2.50	10.50
NI	107.00	7.00	151	9.00	102.00	4.00	4.00	7.00	4.00	3.00
V	189	7.00	157	29.00	176	5.00	5.00	152	5.00	5.00
CR	210	9.00	490	11.00	278	1.00	6.00	1.00	8.00	1.00
GA	nd	nd	nd	nd	nd	nd	nd	nd	nd	nd
CE	66.00	93.00	195	80.00	77.00	152	149	127	143	150
ND	47.00	33.00	103.00	29.00	43.00	66.00	64.00	65.00	62.00	66.00
LA	37.00	50.00	90.00	16.00	43.00	74.00	74.00	56.00	76.00	72.00
TH	6.00	15.00	19.00	16.00	4.00	26.00	22.00	8.00	43.00	25.00
PB	11.00	10.00	19.00	20.00	9.00	27.00	44.00	9.00	22.00	24.00
U	3.00	5.00	6.00	5.00	5.00	7.00	7.00	3.00	3.00	9.00
CU	31.00	4.00	51.00	8.00	34.00	6.00	7.00	6.00	6.00	5.00
ZN	94.00	28.00	98.00	42.00	87.00	115	121	138	24.00	48.00
MG#	63.92	89.02	73.33	49.70	66.96	55.91	26.03	44.67	43.17	27.62
ZR/Y	6.30	6.50	8.63	9.18	7.13	7.39	6.80	4.61	3.08	7.44
K2+NA	3.61	5.23	5.17	7.95	4.55	9.24	9.81	5.90	7.77	9.33
H	238	218	204	.10000	136	974	1192	580	nd	nd
CE/Y	2.44	5.81	5.13	4.71	3.35	2.98	2.76	2.59	2.34	3.00

-118 -   BASALT BW
-119 -   TUFF BW
-120 -   BASALT BW
-122 -   RHYODACITE BW
-123 -   BASALT BW
-132 -   RHYODACITE-R RD1
-137 -   RHYODACITE-B RD1
-150 -   ~~RHYODACITE-B-RD1~~ *BASALT BW*
-151 -   HILTABA GRANITE
-152 -   RHYODACITE-R RD1

APPENDIX 4

Rb-Sr AND Sm-Nd ISOTOPIC DATA

sample no.	908-1 RHYOLITE IGNIMBRITE	908-18 ANDESITE	908-106 DACITE/ RHYODACITE	908-150 BASALT Mg-poor	K5 BASALT Mg-poor
Nd ppm	51.105	33.599			49.775
2 sigma	0.1	0.1			
Sm ppm	8.056	6.133			9.951
2 sigma	0.1	0.1			
143/144 Nd	0.511224	0.511461			0.51169
2 sigma	0.00003	0.00003			
Sm/Nd	0.1576362	0.1825352			0.1999196
147Sm/144Nd	0.0953542	0.1104155			0.1209314
143/144Nd ch	0.512638	0.512638			0.512638
143/144Nd dep	0.513108	0.513108			0.513108
T mod:chur	2.1186222	2.0716708			1.9012465
T mod:dep	2.3751696	2.373431			2.2709361
eps Nd (0)	-27.58282	-22.95967			-18.49258
age (T)	1.59	1.59			1.59
143/144(T)	0.5102273	0.5103068			0.5104259
143/144ch T	0.5106045	0.5106045			0.5106045
eps Nd chT	-7.387811	-5.829548			-3.497423
Sr87/86	0.989861	0.724134	0.754211	0.7146	0.714982
2 sigma	0.00006	0.00006	0.00006	0.00006	0.00006
Sr ppm	43	389	225	491	549
Rb ppm	185	103	166	74	71
Rb/Sr	4.3023256	0.2647815	0.7377778	0.1507128	0.129326
Rb87/Sr86	12.462891	0.7670137	2.1377778	0.4365819	0.37199
87/86(T)	0.7052732	0.7066194	0.754211	0.7146	0.7064877
87/86/300	0.9366558	0.7208596	0.7450846	0.7127362	0.7133939
87/86/400	0.9188704	0.719765	0.7420339	0.7121132	0.7128631
87/86/480	0.9046238	0.7188882	0.7395901	0.7116141	0.7124379
87/86/550	0.8921447	0.7181202	0.7374496	0.7111769	0.7120654
87/86/1000	0.8116255	0.7131647	0.723638	0.7083563	0.7096621

APPENDIX 5

LEAST SQUARES MIXING CALCULATIONS RAW DATA

UNWEIGHTED INPUT DATA:

	PARENT	LAB-15	-123-A	DAUGHTER
SIO2	53.11	55.88	54.46	53.32
TIO2	1.18	0.00	0.26	2.22
AL2O3	15.63	28.78	2.80	14.36
FE2O3	0.00	0.00	0.00	0.00
FEO	8.65	0.96	7.75	10.85
MNO	0.15	0.00	0.17	0.23
MGO	6.16	0.00	18.81	3.36
CAO	8.18	11.01	12.48	6.48
NA2O	2.75	5.43	0.38	2.77
K2O	0.86	0.22	0.00	2.74
H2O+	1.32	0.00	0.00	0.64
H2O-	0.00	0.00	0.00	0.00
P2O5	0.44	0.00	0.00	1.36

(PARENT-MINERALS=DAUGHTER)

PARENT: -118 Basalt
DAUGHTER: -021 Basalt

	SOL'N	% CUMULATE
-118	1.000	
LAB-15	-0.210	53.696
-123-A	-0.181	46.304
-021	0.608	

R SQUARED = 6.312

	PARENT ANALYSIS	DAUGHTER ANALYSIS	DAUGHTER CALC	WEIGHTED RESID
SIO2	54.69	54.58	54.30	0.28
TIO2	1.22	2.27	1.92	0.35
AL2O3	16.10	14.70	15.87	-1.17
FEO	8.90	11.11	11.95	-0.84
MNO	0.15	0.24	0.20	0.03
MGO	6.34	3.44	4.65	-1.21
CAO	8.42	6.63	6.29	0.35
NA2O	2.83	2.84	2.70	0.13
K2O	0.89	2.80	1.38	1.42
P2O5	0.45	1.39	0.75	0.65

UNWEIGHTED INPUT DATA:

	PARENT	-150PI	PL-123	-123 M	Ap-150	-150 I	DAUGHTER
SIO2	53.32	53.55	53.67	0.25	0.53	0.30	70.74
TIO2	2.22	0.00	0.00	0.00	0.00	23.05	0.37
AL2O3	14.36	1.46	28.31	0.20	0.21	0.29	13.84
FE2O3	0.00	0.00	0.00	0.00	0.00	0.00	0.00
FEO	10.85	27.07	1.21	91.47	0.87	71.33	2.76
MNO	0.23	1.13	0.00	0.13	0.00	1.30	0.11
MGO	3.36	12.40	0.22	0.27	0.54	0.26	0.43
CAO	6.48	3.57	11.18	0.12	55.83	0.00	0.81
NA2O	2.77	0.55	5.29	0.35	0.33	0.31	4.26
K2O	2.74	0.16	2.71	0.00	0.00	0.00	5.24
H2O+	0.64	0.00	0.00	0.00	0.00	0.00	0.34
H2O-	0.00	0.00	0.00	0.00	0.00	0.00	0.00
P2O5	1.36	0.00	0.00	0.14	43.19	0.00	0.05

(PARENT-MINERALS=DAUGHTER)

PARENT: -021 Basalt
DAUGHTER: -111 Rhyodacite

	SOL'N	% CUMULATE
-021	1.000	
-150PI	-0.246	36.179
PL-123	-0.349	51.354
-123 M	0.036	-5.287
Ap-150	-0.031	4.567
-150 I	-0.090	13.188
-111	0.320	

R SQUARED =   4.064

	PARENT ANALYSIS	DAUGHTER ANALYSIS	DAUGHTER CALC	WEIGHTED RESID
SIO2	54.58	71.74	72.35	-0.61
TIO2	2.27	0.38	0.41	-0.04
AL2O3	14.70	14.03	14.62	-0.58
FEO	11.11	2.80	2.83	-0.03
MNO	0.24	0.11	-0.50	0.61
MGO	3.44	0.44	0.85	-0.41
CAO	6.63	0.82	0.70	0.12
NA2O	2.84	4.32	2.73	1.59
K2O	2.80	5.31	5.79	-0.48
P2O5	1.39	0.05	0.23	-0.17

UNWEIGHTED INPUT DATA:

	PARENT	-151	K-SP-1	-150 I	Ap-150	DAUGHTER
SIO2	70.74	60.81	65.19	0.30	0.53	76.00
TIO2	0.37	0.00	0.09	23.05	0.00	0.16
AL2O3	13.84	19.45	19.10	0.29	0.21	12.11
FE2O3	0.00	0.00	0.00	0.00	0.00	0.00
FEO	2.76	0.00	0.76	71.33	0.87	1.84
MNO	0.11	0.00	0.00	1.30	0.00	0.06
MGO	0.43	0.00	0.14	0.26	0.54	0.21
CAO	0.81	1.80	0.77	0.00	55.83	0.52
NA2O	4.26	10.71	7.10	0.31	0.33	2.41
K2O	5.24	0.80	5.29	0.00	0.00	5.21
H2O+	0.34	0.00	0.00	0.00	0.00	0.64
H2O-	0.00	0.00	0.00	0.00	0.00	0.00
P2O5	0.05	0.00	0.00	0.00	43.19	0.03

(PARENT-MINERALS=DAUGHTER)

PARENT: -111 Rhyodacite
DAUGHTER: -001 Rhyolite

	SOL'N	% CUMULATE
-111	1.000	
-151	-0.030	8.965
K-SP-1	-0.280	84.941
-150 I	-0.018	5.317
Ap-150	-0.003	0.776
-001	0.670	

R SQUARED =   1.188

	PARENT ANALYSIS	DAUGHTER ANALYSIS	DAUGHTER CALC	WEIGHTED RESID
SIO2	71.74	77.11	76.43	0.68
TIO2	0.38	0.16	-0.10	0.26
AL2O3	14.03	12.29	11.93	0.36
FEO	2.80	1.87	1.93	-0.06
MNO	0.11	0.06	0.13	-0.07
MGO	0.44	0.21	0.58	-0.37
CAO	0.82	0.53	0.61	-0.08
NA2O	4.32	2.45	2.93	-0.48
K2O	5.31	5.29	5.64	-0.36
P2O5	0.05	0.03	-0.09	0.12

UNWEIGHTED INPUT DATA:

	PARENT	AND-15	K-SP-1	-150 A	-150 I	DAUGHTER
SIO2	64.09	55.74	65.19	53.00	0.30	68.00
TIO2	0.98	0.00	0.09	0.29	23.05	0.62
AL2O3	13.90	28.28	19.10	0.77	0.29	13.76
FE2O3	0.00	0.00	0.00	0.00	0.00	0.00
FEO	6.24	0.76	0.76	14.19	71.33	4.27
MNO	0.16	0.00	0.00	0.54	1.30	0.14
MGO	1.59	0.23	0.14	13.36	0.26	1.00
CAO	2.98	10.51	0.77	18.05	0.00	1.93
NA2O	4.05	5.95	7.10	0.29	0.31	3.63
K2O	3.62	0.16	5.29	0.00	0.00	4.43
H2O+	0.85	0.00	0.00	0.00	0.00	0.81
H2O-	0.00	0.00	0.00	0.00	0.00	0.00
P2O5	0.27	0.00	0.00	0.00	0.00	0.16

(PARENT-MINERALS=DAUGHTER)

PARENT: -064 Dacite
DAUGHTER: -105 Rhyodacite

	SOL'N	% CUMULATE
-064	1.000	
AND-15	-0.052	20.677
K-SP-1	-0.113	44.863
-150 A	-0.058	23.170
-150 I	-0.028	11.289
-105	0.749	

R SQUARED = 0.399

	PARENT ANALYSIS	DAUGHTER ANALYSIS	DAUGHTER CALC	WEIGHTED RESID
SIO2	65.46	69.43	69.58	-0.15
TIO2	1.00	0.63	0.40	0.24
AL2O3	14.20	14.05	14.04	0.00
FEO	6.37	4.36	4.45	-0.08
MNO	0.16	0.14	0.13	0.02
MGO	1.62	1.02	1.09	-0.07
CAO	3.04	1.97	1.83	0.14
NA2O	4.14	3.71	4.00	-0.29
K2O	3.70	4.52	4.12	0.40
P2O5	0.28	0.16	0.37	-0.21

GEOLOGY OF THE KOKATHA REGION, GAWLER RANGES, SOUTH AUSTRALIA

LEGEND

CAINOZOIC

- CAINOZOIC SEDIMENTS

MIDDLE PROTEROZOIC (CARPENTARIAN)

- HILTABA GRANITE

CYCLE 2

- CHANDABOOKA DACITE D1
- VOLCANICLASTIC VL5
- RHYOLITE RH5
- DACITE TBD
- DACITE GMD
- VOLCANICLASTIC VL4
- Brecciated RHYOLITE/RHYODACITE UNIT RH4
- ANDESITE AE
- FLOW-BANDED RHYOLITE FRH
- VOLCANICLASTIC VL3
- BASALT BE

CYCLE 1

- EPICLASTIC VL2
- EPICLASTIC TU4
- RHYODACITE RU1
- VOLCANICLASTIC VL1
- AIR FALL TUFF TU3
- FLOW-BANDED RHYODACITE FR1
- RHYODACITE BGD
- RHYOLITIC BRECCIA FLOW BF
- RHYOLITE IGNIMBRITE RH3
- RHYOLITE IGNIMBRITE RH2
- RHYOLITE IGNIMBRITE RH1
- AIR FALL TUFF TU2
- RHYODACITE UNIT RD2
- AIR FALL TUFF TU1
- RYODACITE UNIT RD1
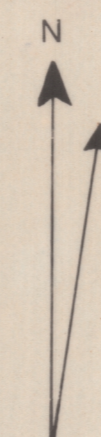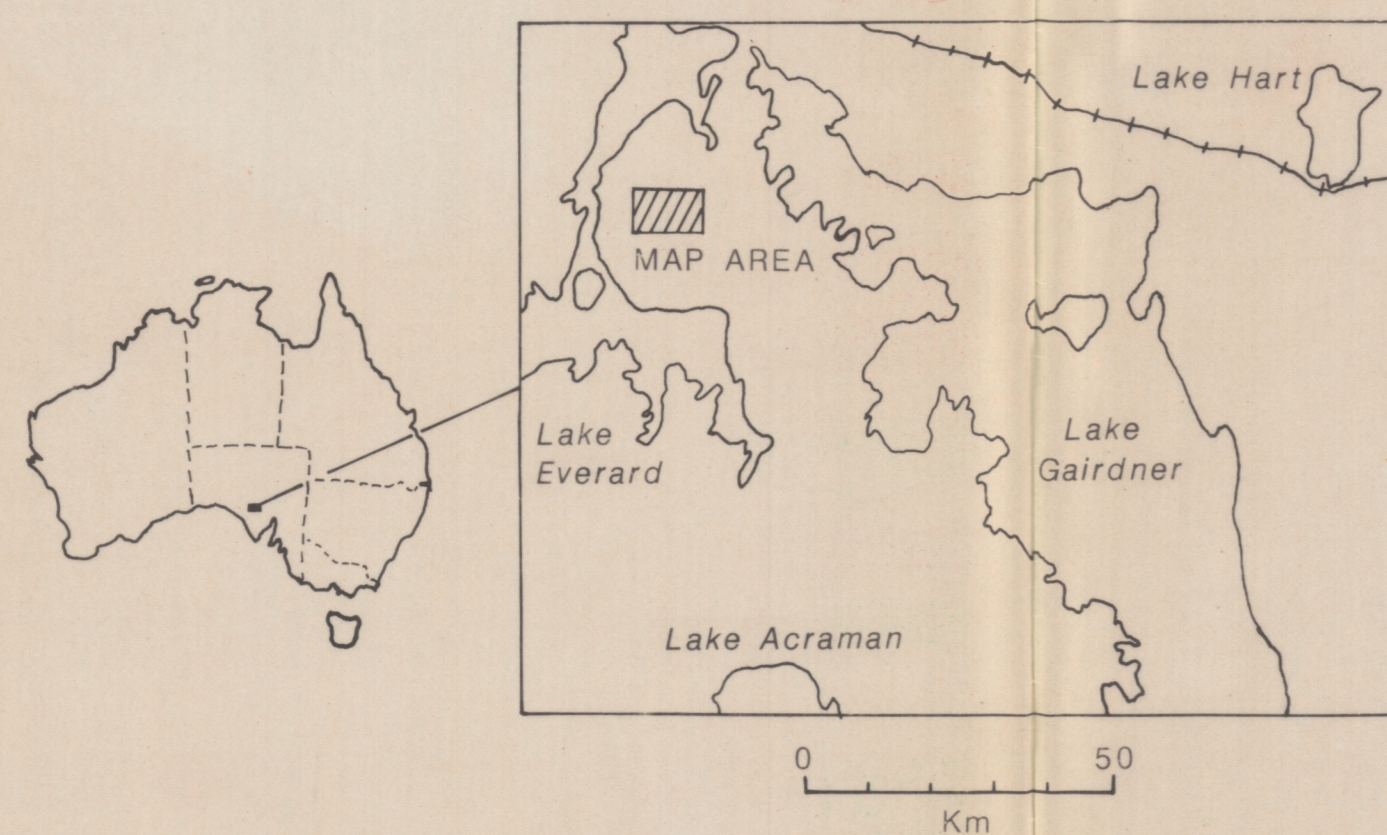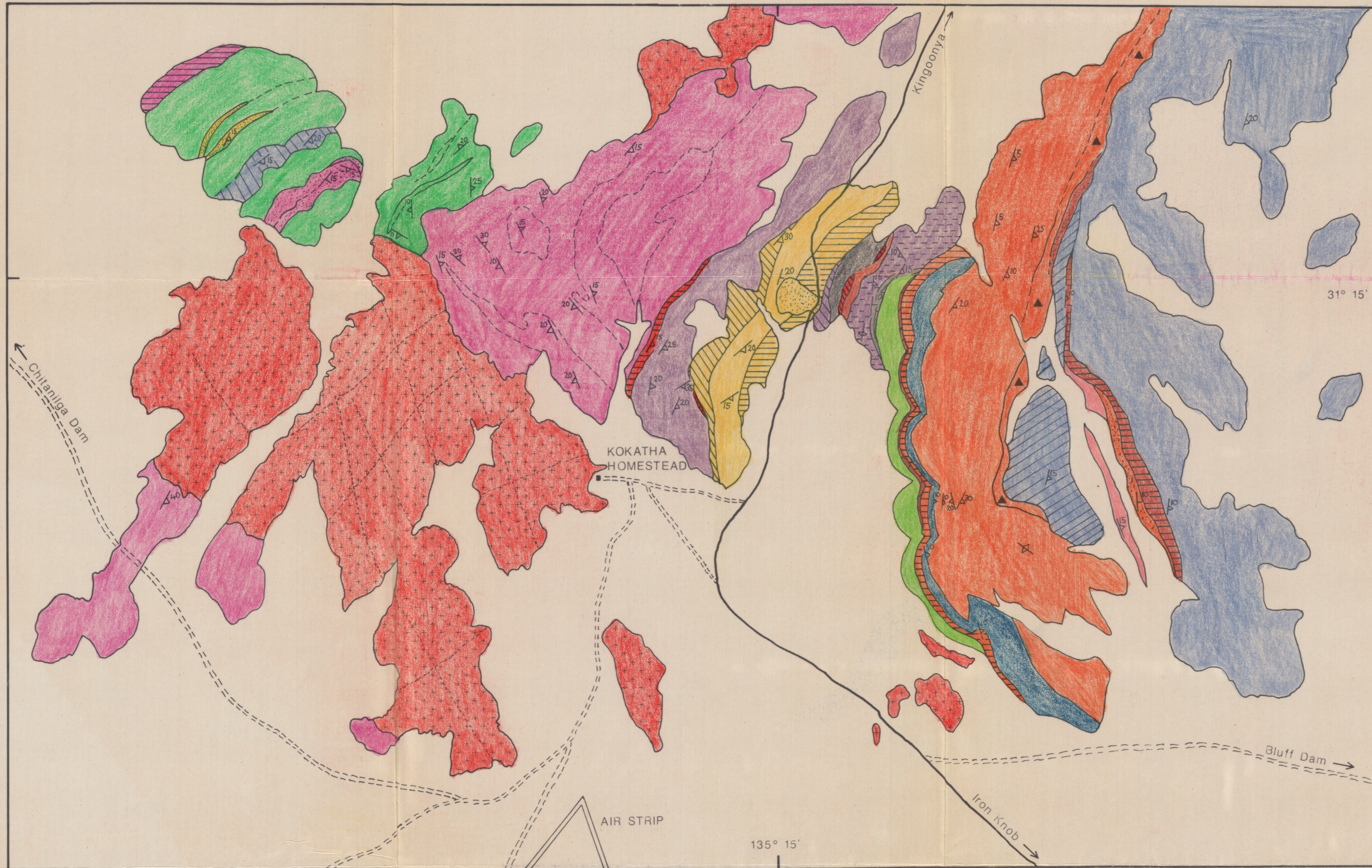- BASALT BW
- RHYODACITE BW2
- BASALT BW
- DACITE BW
- BASALT BW (WITH RHYOLITIC TUFFS)
- RHYODACITE BW1

SCALE 1:20000

0 500 1000 1500 2000

METRES

GAIRDNER SHEET SH53-15

MAP AREA

Lake Hart
Lake Everard
Lake Gairdner
Lake Acraman

0   50
Km

N

GEOLOGICAL BOUNDARY

———— OBSERVED

- - - - INFERRED

FLOW BANDING

⟋20 INCLINED

⊘ VERTICAL

BEDDING

⟋20 INCLINED

~~ ROAD

-·-·- VEHICLE TRACK

╬ JOINT SETS

Kingoonya
Chitanilga Dam
KOKATHA HOMESTEAD
31° 15'
135° 15'
Bluff Dam
Iron Knob
AIR STRIP

B. Robertson, 11/89